The synthesis and characterization of the ZnO nanoparticles

by

Tshabalala Modiehi Amelia

(B.Sc Hons)

A dissertation presented in fulfilment of the requirements for the degree

MAGISTER SCIENTIAE

in the

Faculty of Natural and Agricultural Sciences

Department of Physics

at the

University of the Free State, (Qwa Qwa Campus)

Republic of South Africa

Supervisor: Prof. B. F. Dejene

Co-supervisor: Prof. H. C. Swart

November 2011

UNIVERSITY OF THE
FREE STATE
UNIVERSITEIT VAN DIE
VRYSTAAT
YUNIVESITHI YA
FREISTATA

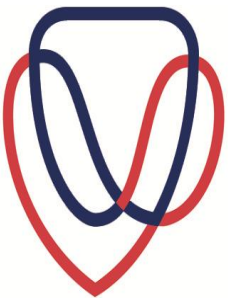

UFS
UV

Dedicated to the memory of my late mother

Matshidiso Elizabeth Tshabalala

(1943-2012)

He is the creator of mankind.

Acknowledgements

My utmost gratitude to the almighty, creator of all things, the one who really controls weather i have my tomorrow on not.

My sincere thanks and gratitude go to:

- My supervisor, ***Prof. B.F. Dejene*** for his patience, dedication and understanding and all the work we have done together. He has shown a fatherly love throughout the study, gave me advices on many things, and held my hand through and through.

- My co-supervisor, ***Prof. H.C Swart*** for his useful comments, patience and his valuable suggestions.

- South African National Research Foundation (NRF) and the University of the Free State (UFS) for financial support.

- A great thank you to ***Mr L.F. Koao*** for his suggestions and his help and making me learn what research is about.

- A big thank you to UFS Physics Department (QwaQwa campus) staff and postgraduate students ***(Ms. M.A. Lephoto, Ms K.E. Foka, Mr A.G. Ali, Mr M Mbongo, Mr A.H. Wako)*** for their inputs during this study.

- Thank you to my fellow researchers in UFS (Bloemfontein campus), ***Mrs M.M Duvenhage*** for her unfailing support, patience and holding my hand through the characterization, ***Ms. P.S Mbule*** and ***Mr Hassan*** for their support during the PL data.

- ***Prof. JR Botha and his student (Julien)***, Physics department, University of Port Elizabeth, for allowing me to use their research facilities (PL measurement) at NMMU and for helping with the analysis of PL results.

- ***Mr. Motaung T.E*** at Chemistry Department (QwaQwa campus) for his unwavering help by borrowing me the necessary apparatus during the synthesis and preparation of the samples.

- ***Dr Bem D.B*** for his none exhausting help during the period of this research and for his support.

Abstract

ZnO has been by far the most interesting semiconductor because of its properties. The ZnO nanostructures were synthesized by a sol-gel method and the samples were annealed in air at various temperatures capped with polymers PVP (Polyvinyl Pyrrolidone) and PEG (Polyethylene glycol). Again the ZnO was synthesized using different solvents; ethanol, methanol or water at various temperatures. Characterizations of the powders were carried out using different techniques. The structure and the particle size of the samples were obtained using the XRD (x-ray diffraction). The morphology was determined by the SEM (scanning electron microscopy) and the chemical composition was analyzed using the EDS (energy x-ray dispersed spectroscopy). The PL (photoluminescence) data were collected using the He-Cd (Helium-Cadmium) laser and also using the Cary Eclipse fluorescence spectroscopy at room temperature. The absorption spectra were analyzed using the UV-Vis spectroscopy.

The PL spectra for the ZnO nanostructures capped and prepared using polymers showed broad emissions in the visible range. The broad emission in the visible range with maximum intensity peaks at 449 nm and at 530 nm for the PVP capped ZnO nanoparticles were observed annealed at 150°C. This was influenced by the addition of various molar masses of PVP on the $Zn(Ac)_2$. The green emission band at 560 nm and a blue emission at 450 nm were obtained for the PEG encapsulated ZnO nanostructure. The PL of the ZnO nanoparticles prepared using various solvent was shown, the different shifts from the emission peaks were observed and the fluctuation of the intensity which was attributed to an increase and a decrease on the annealing temperatures. The effect of pH values on the ZnO prepared using different solvents. The PL on these samples exhibited a strong broad blue emission, for all the ZnO prepared using ethanol, methanol or water as solvents. The intensities differed with the amount of NaOH which was added onto the $Zn(Ac)_2$ solution.

The XRD pattern for all the prepared ZnO nanostructures exhibited the peaks corresponding to that of various planes of ZnO wurtzite structure with the JCPDS (Joint Committee on Powder Diffraction Standards) file no. (13-1451). The absorption spectra of the PVP capped ZnO nanostructures did not show any shifts while the absorption spectra for the PEG encapsulated ZnO nanostructures showed a shifts with an addition of the molar masses of the PEG. The UV-Vis spectroscopy for the ZnO prepared with ethanol, methanol or water as solvents at various temperatures gave the absorption edges and also the blue shifts that

occurred with and increase on the annealing temperatures 300, 400, 500 and 600°C. It was observed from the UV absorption of the ZnO using different solvents with various pH values that the band gaps for all the samples were determined to be larger than that of ZnO bulk. The NaOH solution which was slowly added on the $Zn(Ac)_2$ solution took control over the surface of the ZnO surfaces.

Keywords

ZnO, PEG, PVP, Methanol, ethanol, water, pH

Acronyms

- PVP - Polyvinyl Pyrrolidone
- PEG - Polyethylene glycol
- PL - Photoluminescence
- XRD - X-ray diffraction
- UV - Ultra violet
- SEM - Scanning electron microscopy
- EDS/EDX - energy x-ray dispersive spectroscopy
- EtOH - Ethanol
- MEtOH - Methanol
- CBD - Chemical Bath Decomposition

Table of Contents

List of figures

CHAPTER 1

INTRODUCTION

1.1. Background

The unique and fascinating properties of group II-VI compound semiconductors have triggered tremendous motivation among the world scientists to study semiconducting nanoparticles. This is because it gives the opportunity to understand the physical properties in low dimensions and to explore their vast potential applications e.g. in optoelectronics. Several oxide nanoparticles are produced with possible future applications, among them zinc oxide with a formula ZnO is considered to be the best one to be exploited at nano-dimensions. Being interestingly important for its ultra violet absorbance, wide chemistry, piezoelectricity and luminescence at high temperatures, ZnO has penetrated into the industry, and one of critical building blocks in today's modern society [1]. However, it has entered the scientific spotlight for its semiconducting properties [2]. This latter in particular based on the large variations of the band gap and type of defect as a function of particle size and synthesis conditions respectively. Moreover, small nanoparticles allow the study of relevant surface properties due to the high surface to bulk ratio. In comparison with the bulk semiconductor, nanoparticles possess many special properties such as ultrafast optical nonlinear response, photo electricity switch and piezoelectric properties. Recently, the preparation of some semiconductor nanoparticles including CdSe, CdS and ZnS has been quite perfect [1-4]. However, there has not been an equivalent success in the synthesis of metal oxides nanoparticles such as ZnO nanoparticles because of the complexity of hydrolyzation in metal ion. ZnO nanoparticles do not only have merits of ZnO semiconductor material such as a large exciton binding energy of 60meV and excellent stability, but also have novel characteristics of particularity of nanostructure [5]. Zinc oxide is an inorganic compound and an n-type semiconductor with unique properties and as an n-type semi conductive materials, it can absorb infrared light and infrared electromagnetic wave with the value of 5 to 16.68 dB in the range of 2.45 to 18 GHz [6]. Firstly, ZnO has high thermal and chemical stability,

which plays an important role in material chemistry and nanotechnology and secondly, it is one of the few oxides that show quantum confinement effects, allowing a fine-tuning of the band gap in an experimentally accessible size range [7]. The confinement effect is obtained in ZnO when the particle sizes are equal or less than 0.7 Å. It is well known that small particles have the large surface-to-volume ratio and surface defects [5]. With a wide band gap of 3.2 eV and a large exciton binding energy of 60 meV at room temperature, ZnO, line GaN, will be important for blue and ultraviolent optical devices and ZnO has several advantages over GaN in this applications range however, the most important being its longer exciton binding energy and the ability to grow single crystal substrates [8]**.** Due to its wide band gap and binding energy, ZnO has attracted properties for optoelectronics, such as superior UV emission characteristics and high stability [9]. It is attractive for forming various forms of nanostructures, such as nanorods, nanowires, and nanobelts. Semiconductor nanomaterials are receiving much attention owing to their novel optical and electronic properties for application in the fields of solar cells, microelectronics, catalysis, optical communications and light emitting diodes [10]. The optoelectronic properties of material are sensitive to its crystal perfection and surface morphology.

The unique properties of nanomaterials have motivated the researchers to develop many simpler and inexpensive techniques to produce nanostructures of technologically important materials. The size range that hold so much interest in nanomaterials is typically from 100 nm down to the atomic level (approximately 0.2 nm), because it is in this range that materials can have different or enhanced properties compared with the same materials at a larger size (bulk) [11]. The nanoscience and technology deal with particles with diameter of 1 to 100 nm, or about 10 to 10^6 atoms or molecules per particle. Because of the small particle size, the materials have very large surface area to volume ratio, bringing out new physical and chemical properties which are different with their larger scale counterparts [7]. An increase on the relative surface area and dominance of quantum confinement effects of charge carriers (electrons and holes) in the restricted volume of nanoparticles are the two main reasons for this change in behaviour [11].

Various processes have been employed to synthesize the ZnO nanostructures, such as electrochemical deposition [12], hydrothermal [13], sputter deposition technique [14], and vapour method [15]. The sol-gel process using zinc acetate [$Zn(CH_3COO)_2.\ 2H_2O$] has

proven to be a relatively simple method for synthesizing of ZnO nanoparticles with a narrow size distribution and excellent crystallinity [16].

The sol-gel process is a wet-chemical technique widely used in the fields of materials science and ceramic engineering [17]. The term sol-gel refers to a process for making glass with additives and sol-gel glasses are of current interest because of their potential applications such as electronics and optics [18]. The process involves the generation of colloidal suspensions (sols) at relatively low temperature, which are subsequently converted into viscous gels [19]. At the transition, the solution or sol becomes a rigid, porous mass through destabilization, precipitation, or super saturation. Sols are dispersions of colloidal particles in a liquid [20] and colloids are solid particles with diameters of 1-100 nm. Sol-gel materials provide an excellent vehicle for the incorporation of secondary phase including metal ions, organic molecules or macromolecules. These species may be doped into the gel-matrix as it is being formed (pre-doping) or incorporated after the glass has been prepared (post-doping) [18].

The sol-gel process was also used in encapsulation of the two polymers PVP and PEG onto the ZnO nanostructures. PVP has been shown a much interest in all the conjugated polymers because of its excellence on the transparency, easy processing situation and the good environmental stability [21]. It was reported that PVP can effectively prevent the ZnO nanoparticles from aggregating and the crystallization of the ZnO nanoparticles can be improved by PVP-modification [22]. Many morphologies of ZnO have been fabricated using the PEG as a polymer surfactant [23]. Synthesizing of the 1-D ZnO nanorods or nanowires, Li et al. [24] have prepared ZnO nanowires or nanorods in the presence of PEG with different molar weight and analyzed the mechanism from the point of ZnO self-growth behaviour and energy decreased.

1.2 Aim of the study

The objective of this study:

- ✓ The difference on the properties of the ZnO nanoparticles using the Sol-gel process, with different molar masses of the polymers: PVP, and PEG as the capping agents. To

investigate the optical properties and the morphology of the ZnO capped with these polymers.

- ✓ The synthesis and the characterization of the ZnO prepared with different solvents: methanol, ethanol, and water to investigate the effect of these solvents on the ZnO nanoparticles.

- ✓ The effect of pH levels on the preparation of the ZnO, and the temperature effect on the nanoparticles.

1.3 Problem of statement

ZnO semiconductor nanostructures are attractive components for nanometre scale electronic and photonic device applications because of their unique chemical and physical properties. ZnO nanostructures have also attracted considerable attention with great potential for overcoming fundamental limitations due to their ultrahigh surface to volume ratio. For example, recently, a wide variety of nanodevices including ultraviolet photodetectors, photovoltaic, sensors, field effect transistors , intramolecular p-n junction diodes, Schottky diodes and light emitting device arrays have been fabricated utilizing ZnO nanorods (nanowires). Although a range of interesting properties are associated with ZnO nanorods (or nanowires), in the context of various intriguing applications, there are also some challenges remaining. The first challenge faced by the current synthesis methods of ZnO nanostructures is the ability to control its morphology and self-assembly into complex structures or device architectures. The second is to grow p-type ZnO nanostructures. The third challenge is to demonstrate radically new applications for ZnO nanorod-based nanostructures. In my opinion, ZnO could be one of the most important nanomaterials in future research and applications.

1.4 Thesis Layout

In this thesis there are seven chapters.

Chapter 1 is the introduction of the ZnO and theory behind.

- In this chapter, ZnO is being introduced. The characteristics it has and the shapes that it can be prepared into.

Chapter 2 gives the literature review and the different properties of the ZnO and the method used during the synthesis.

- The methods used and properties of the ZnO are discussed in this chapter. The properties included the structure, electrical and optical properties. The method which was used in this investigation is also discussed in detail.

Chapter 3 investigates the theory behind the techniques which were used in this project.

- The techniques which were used in this thesis are reported. The attention was mainly on the inside of the techniques. How they operate in order to have results that were discovered.

Chapter 4 deals with the synthesis and characterization of the ZnO nanoparticles using PEG.

- The preparation of the ZnO encapsulated with PEG is discussed in this chapter. The impact that the PEG has on both structure and the optical properties of the ZnO. The results on this preparation were also observed using various techniques which were discussed in chapter 3.

Chapter 5 Synthesis and characterization of the ZnO nanoparticles and the PVP encapsulated ZnO nanoparticles.

- The influence that the PVP has brought on the morphology of the ZnO nanoparticles, both encapsulated and not capsulated.

Chapter 6 Comparison of ZnO nanoparticles properties synthesised using various solvents.

- ZnO in this chapter has been prepared with different solvents. The aim here was to observe the effect that the water, ethanol and methanol has on the ZnO luminescence properties and structure. These ZnO powders were calcined at different temperatures,

therefore the impact on the temperatures was also observed. The lattice parameters and the crystallite size were calculated using the Braggs equation and the Scherer equation.

Chapter 7 The control of the pH level during the synthesis and characterization of the ZnO nanoparticles.

- Different pH levels have been taken on the preparation of the ZnO nanoparticles. In this chapter the temperature was kept constant with variation on the pH. What was observed is that this (pH) has brought change on the structure and the particle size of the ZnO.

Chapter 8 is the conclusion of what has been happening on the project and has been achieved during the preparation.

- Conclusion and summary of what has been discussed in this report and what will be the future work.

References

[1] Ü. Özgür, Ya. I. Alivov, C. Liu, A. Teke, M. A. Reshchikov, S. Doğan, V. Avrutin, S.J. Cho and H. Morkoçd, *J. Appl. Phys.* **98** 041301 (2005)

[2] C. Jin "Growth and characterization of ZnO and ZnO-based Alloys-$Mg_xZn_{1-x}O$ and $Mn_xZn_{1-x}O$" PhD thesis, Department of materials science and Engineering, North Carolina state university, Raleigh (2003)

[3] G. Ferblantier, F. Mailly, R. Al Asmar, A. Foucaran, F. Pascal-Delannoy, *Sensor and Actuators* A **122** 184-188 (2005)

[4] S. J. Pearton, D. P. Norton, K. Ip, Y. W. Heo, T. Steinerb, *Super lattices and Microstructures* **34** 29-32 (2003)

[5] G. Ali, MSc Thesis, University of the Free State, Republic of South Africa (2009)

[6] J. Cheng, X. Zhang, X. Tao, and F. Liu, *Conference on Nano/Micro Engineered and Molecular System* **497** 18-21 (2006)

[7] http://ubm.opus.hbz-nrw.de/volltexte/2007/1222/pdf/diss.pdf [05 September 2011]

[8] http://www.intechopen.com/source/pdfs/11911/InTech Growth_of_undoped_and_metal_doped_zno_nanostructures_by_solution_growth.pdf [05 September 2011]

[9] R. Brayner, S. A. Dahoumane, C. Yéprémian, C. Djediat, M. Meyer, A. Couté, F. Fiévet, *Langmuir*, 26 (**9**) 6522-6528 (2010)

[10] L. Shen, N. Bao, K. Yanagisawa, K. Domen, A. Gupta and C. A. Grimes, *Nanotechnology*, **17** 5117-5123 (2006)

[11] Nanoscience and technologies, available from www.nanotec.org.uk/report/chapter2.pdf [08 September 2011]

[12] G. R. Li, D. L. Qu, W. X. Zhao, Y. X. Tong, *J. Mater. Chem.* **9** 1661-1666 (2007)

[13] K. H. Tam, et al., *J. Phys. Chem. B* **110** 20865-20871 (2006)

[14] W. T. Chiou, W. Y. Wu, J. M. Ting, *Diamond Relat. Mater.* **12** 1841-1844 (2003)

[15] Y. Zhang, K. Yu, D. Jiang, Z. Zhu, H. Geng, L. Luo, *Appl. Surf. Sci.* **242** 212-217 (2005)

[16] Y. L. Zhang, Y. Yang, J. H. Zhao, R. Q. Tan, P. Cui, W. J. Song, *J. Sol-Gel Sci. Technol*, **51** 198-203 (2009)

[17] http://en.wikipedia.org/wiki/Sol-gel [07 September 2011]

[18] Koao L. F., MSc thesis, University of the Free State, Republic of South Africa, (2009)

[19] O. M. Ntwaeaborwa, PhD Thesis, University of the Free State, Republic of South Africa, (2006)

[20] L. L. Hench, J. K. West, *Chem. Rev*., **90** 33-72 (1990)

[21] K. Sivaiah, B. H. Rudramadevi and S. Buddhudu, *Indian J. Of Pure & Appl. Phys.*, **48** 658-662 (2010)

[22] H. Tang, M. Yan, X. Ma, H. Zhang, M. Wang, D. Yang, *Sensors and Actuators B* **113** 324-328 (2006)

[23] Y. Feng, M. Zhang, M. Guo, X. Wang, *Crystal Growth Design Article*, **10** 1500-1507 (2010)

[24] Z. Q. Li, Y. J. Xiong, Y. Xie, *Inorg. Chem.* **42** 8105-8109 (2003)

CHAPTER 2

LITERATURE REVIEW

After silicon and germanium, ZnO was one of the first semiconductors to be prepared in a pure form. It was extensively characterized as early as the 1950`s and 1960`s due to its promising piezoelectric/acoustoelectric properties [1]. In the past 100 years, it has featured as subject of thousands of research papers, dating back as early as 1935 [2]. ZnO is an n-type semiconductor with unique properties such as transparency in the visible and high infrared reflectibly acoustic characteristics, high electrochemical stability and excellently electronic properties [3]. Wide band gap semiconductors have gained much attention during last decade because of their possible uses as optoelectronic devices in the short wavelength and ultraviolet (UV) portion of the electromagnetic spectrum. Semiconductors such as ZnSe, ZnS, SiC, GaN, SnO_2 and ZnO, have shown similar properties with their crystal structures and band gaps [1]. Table 2.1 shows the comparison of different semiconductors. Recently, it has been introduced that ZnO as II–VI semiconductor is promising for various technological applications, especially for optoelectronic short wavelength light emitting devices due to its wide and direct band. This attraction can simply be attributed to the large exciton binding energy of 60 meV of ZnO potentially paving the way for efficient room-temperature exciton-based emitters, and sharp transitions facilitating very low threshold semiconductor lasers [4]. Since ZnO and GaN have almost identical lattice parameters and the same hexagonal wurtzite structure, ZnO can satisfactorily be used as lattice matched substrate in GaN based devices or vice versa. ZnO has excellent radiation hardness among all other semiconductors. This property supplies the uses of ZnO based devices in space applications and high energy radiation environments. Band gap energy can be varied from 3.3 eV up to 4.5 eV with alloying process. Hence it can be used as an active layer in the doubly confined hetero-structured LEDs and quantum well lasers. These unique nanostructures unambiguously demonstrate that ZnO is probably the richest family of nanostructures among all materials, both in structure and properties [5]. The properties of the ZnO depend closely on the

microstructures of the materials, including crystal size, orientation and morphology, aspect ratio, and even crystalline density [6].

This is one of the key parameter that ZnO exhibits near-UV emission, transparency, conductivity, and resistance to high temperature electronic degradation [7] and holds excellent promise for blue and ultra-violet optical devices. Although in the past GaN and GaN-based materials have dominated this wavelength range, ZnO enters the arena with several advantages [2]. The two most crucial of these are:

(a). The larger exciton binding energy, which will allow for room temperature devices operating with higher efficiency and lower power threshold for lasing by optical pumping.

(b). The ability to grow high quality single crystal substrates with relative cost effectiveness and ease - something that still eludes GaN that highlights some of the key properties of ZnO, and provides a comparison with GaN. Other favourable aspects of ZnO include its broad chemistry leading to many opportunities for wet chemical etching, piezoelectric properties, radiation hardness and high ferromagnetic Curie temperature for spintronic applications [2].

2.1 Comparison of different semiconductors

ZnO was one of the first semiconductors to be prepared in rather pure form after silicon and germanium. It was extensively characterized as early as the 1950's and 1960's due to its promising piezoelectric/acoustoelectric properties. Wide band gap semiconductors have gained much attention during last decade because of their possible uses as optoelectronic devices in the short wavelength and ultraviolet (UV) portion of the electromagnetic spectrum. These semiconductors such as ZnSe, ZnS, GaN, and ZnO, have shown similar properties with their crystal structures and band gaps. As shown in table 2.1, some of the important properties of these wide band gap semiconductors are summarized. Initially, ZnSe based devices and the GaN based technologies obtained large improvements such as blue and UV light emitting diode and injection laser. ZnSe has produced some defect levels under high current drive. No doubt, GaN are considered to be the best candidate for the optoelectronic devices. However, ZnO has great advantages for light emitting diodes (LEDs) and laser diodes (LDs) over the currently used semiconductors. Recently, it has been introduced that ZnO as II–VI semiconductor is promising for various technological applications, especially for optoelectronic short wavelength light emitting devices due to its wide and direct band gap.

The most important advantage is the high exciton binding energy (60 meV) giving rise to efficient exitonic emission at room temperature. Since ZnO and GaN have almost identical lattice parameters and the same hexagonal wurtzite structure, ZnO can satisfactorily be used as lattice matched substrate in GaN based devices or vice versa. ZnO has excellent radiation hardness among all other semiconductors. This property supplies the uses of ZnO based devices in space applications and high energy radiation environments. Band gap energy can be varied from 3.3 eV up to 4.5 eV with alloying process. Hence it can be used as an active layer in the doubly confined hetero-structured LEDs and quantum well lasers. These unique nanostructures unambiguously demonstrate that ZnO is probably the richest family of nanostructures among all materials, both in structure and properties [8].

TABLE 2.1: Comparison of different semiconductors [1].

Wide band gap semiconductors	Crystal structure	Lattice parameters (Å)		Effective mass (me)		Eg (eV at RT)	Melting temperature (K)	Exciton binding energy (meV)	Dielectric constant	
		a	b	m_e	m_h				ε_0	ε_∞
ZnO	Wurtzite	3.250	5.206	0.318	0.50	3.37	2248	60	8.75	3.72
GaN	Wurtzite	3.189	5.185	0.2	0.80	3.4	1973	21	9.5	5.15
ZnSe	Zinc-Blende	5.667	–	0.15	0.78	2.7	1790	20	7.1	5.3
ZnS	Wurtzite	3.824	6.261	0.34	1.76	3.7	2103	36	9.6	5.7
6H-SiC	Wurtzite	3.08	15.12	0.42	1.00	3.0	>2100	–	9.66	6.52
SnO_2	Tetragonal rutile	4.737	3.185	0.1	–	3.6	>2200	32.76	9.65	–

TABLE 2.2 Physical properties of wurzite ZnO [9].

Properties	**Values**
Lattice constant	
a_0	0.34296nm
b_0	0.52096nm
Density	5.6 g/cm^3
Melting point	2248K
Relative dielectric constant	8.66
Gap energy	3.4 eV, direct
Intrinsic carrier concentration	$<10^6$ cm^{-3}
Exciton binding energy	60 meV
Electron effective mass	0.24
Electron mobility	200 cm^2/V.s
Hole effective mass	0.59
Hole mobility	5-50 cm^2/V.s

2.2 Structure

Structurally, ZnO has a non-centrosymmetric wurtzite crystal structure with polar surfaces [7]. The wurtzite structure is most stable at ambient conditions and thus most common. The crystal can be described as alternating planes composed of tetrahedrally coordinated O^{2-} and Zn^{2+} ions, stacked along the c-axis [9]. The hexagonal wurtzite structure (Figure 2.1) has a point group 6 mm or C_{6v} (Schoenflies notation), and the space group is $P6_3mc$ or C_{6v}. The lattice constants are a = 3.25 Å and c = 5.2 Å; their ratio c/a ~ 1.60 is close to the ideal value for hexagonal cell c/a = 1.633 [10]. The physical properties of ZnO semiconductors are presented in Table 2.2.

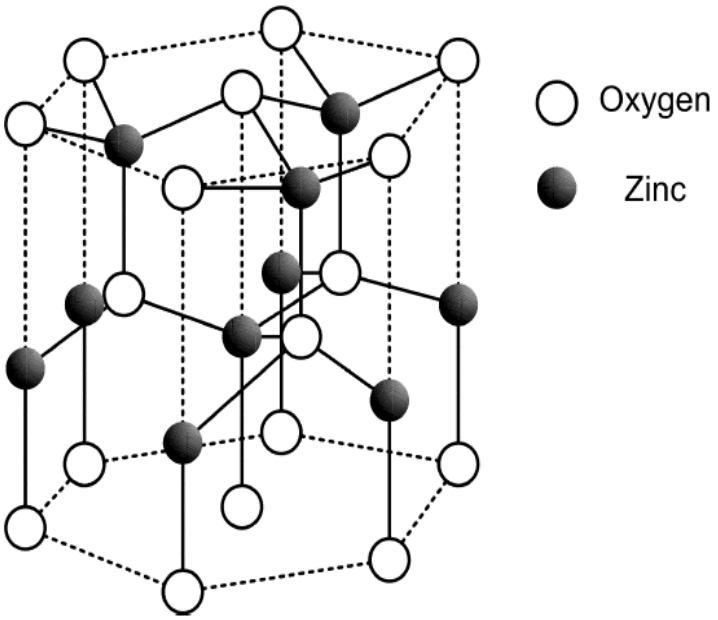

Figure 2.1: ZnO wurtzite structures [9].

2.3 Electrical and optical properties of ZnO

2.3.1 Electrical Properties

ZnO usually exhibits n-type conductivity. Intrinsic defects such as zinc interstitials (Zn_i) or oxygen vacancies (V_O) have been claimed to be accountable for n-type conductivity [11]. The contribution of oxygen vacancies to conductivity has been controversial. Theoretical calculations pointed out those oxygen vacancies are deep donors rather than shallow donors [12]. As a direct and wide band gap semiconductor with a large exciton binding energy (60meV), ZnO is representing a lot of attraction for optoelectronic and electronic devices. For example, a device made by material with a larger band gap may have a high breakdown voltage, lower noise generation, and can operate at higher temperatures with high power operation. The performance of electron transport in semiconductor is different at low and high electric field [1].

When the electrical field is increased, the energy of the electrons from the applied electrical field is equivalent to the thermal energy of the electron. The electron distribution function changes significantly from its equilibrium value. These electrons become hot electrons, whose temperature is higher than the lattice temperature. So there is no energy loss to the

lattice during a short and critical time. When the electron drift velocity is higher than its steady-state value, it is possible to make a higher frequency device.

2.3.2 Optical properties

ZnO is a wide band gap semiconductor that displays luminescent properties in the near ultra violet and the visible regions, and the emission properties of ZnO nanoparticles in the visible region widely depend on their synthetic method as they are attributable to surface defects [13]. The high efficiency of luminescence in the UV to visible regions of the spectrum makes ZnO an attractive material for optoelectronic applications. The near-band gap emission is due to recombination of free electrons in the conduction band and holes in the valence band. A broadband emission within the visible region, due to transitions involving defect states, is a common photoluminescence feature of bulk ZnO [14]. Impurity atoms also contribute to visible emission; e.g., green luminescence from Cu acceptors in ZnO [15].

The optical properties of a semiconductor are associated with both intrinsic and extrinsic effects. Intrinsic optical transitions take place between the electrons in the conduction band and holes in the valence band, including excitonic effects due to the Coulomb interaction. The main condition for exciton formation is that the group velocity of the electron and hole is equal. Excitons are classified into free and bound excitons. In high quality samples with low impurity concentrations, the free exciton can also exhibit excited states, in addition to their ground-state transitions. Extrinsic properties are related to dopants or defects, which usually create discrete electronic states in the band gap, and therefore influence both optical-absorption and emission processes [1].

2.4 Sol-gel Process

The sol-gel process (see figure 2.2), as the name implies, involves the evolution of inorganic networks through the formation of a colloidal suspension (sol) and gelation of the sol to form a network in a continuous liquid phase (gel) [16]. The sol-gel is one of the most suitable ways for producing glasses and glass nanoparticles. As an alternative to melted glass, a sol-gel derived glass is a good medium for studying crystallization and phase separation [17]. The relatively mild reaction conditions, purity, homogeneity and simplicity of the sol-gel method make it an excellent tool for producing substances with precisely tailored properties [18]. The

sol-gel technique is one of the fastest growing fields of contemporary chemistry. The main advantage of this process stems from the fact that it offers an alternative approach to conventional production of glasses, glass-like materials and ceramics of various properties and applications [19].

The production of glasses by the sol-gel method permits preparation of glasses at far lower temperatures than is possible by using conventional melting. It also makes possible synthesis of compositions that are difficult to obtain by conventional means because of problems associated with volatilization, high melting temperatures, or crystallization. In addition, the sol-gel approach is a high-purity process that leads to excellent homogeneity. Finally, the sol-gel approach is adaptable to producing films and fibers as well as bulk pieces [20]. The sol-gel process can be characterized by a series of distinct steps which are gelation, drying and densification [21].

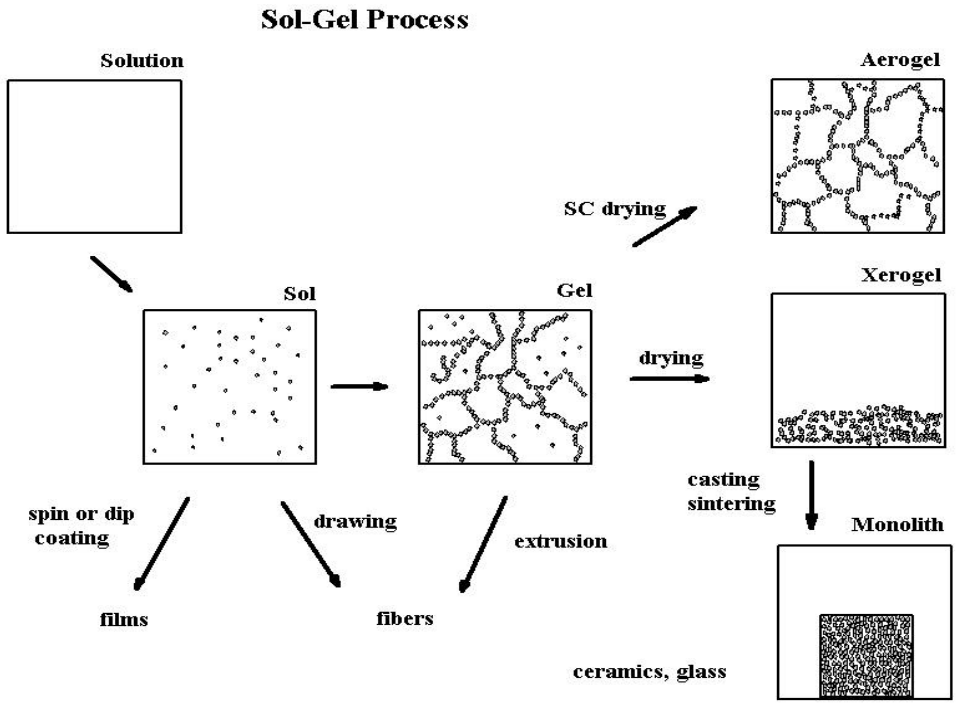

Figure 2.2: Schematic representation of the sol-gel process [25].

Materials obtained by the sol-gel-process, in which covalent organic groups can be integrated into an inorganic network, are referred to as inorganic-organic composites. These are obtained by hydrolysis and condensation reactions, for example, based on modified silicon alkoxides. The alkoxide used most often to synthesize SiO_2 is tetraethylorthosilicate (TEOS),

which is the product of the reaction of $SiCl_4$ and ethanol [22]. Precursors may be dissolved in organic or aqueous solvents and catalysts are often added to accelerate hydrolysis and condensation reactions. A silica gel may be formed by the network growth from an array of discrete colloidal particles or by formation of an interconnected 3-D network by the simultaneous hydrolysis and polycondensation of an organometallic precursor [23]. A liquid alkoxide precursor such as $Si(OR)_4$, where R may be CH_3, C_2H_5, or C_3H_7 is hydrolyzed by mixing with water to form hydrated silica and alcohol as shown below.

Hydrolysis

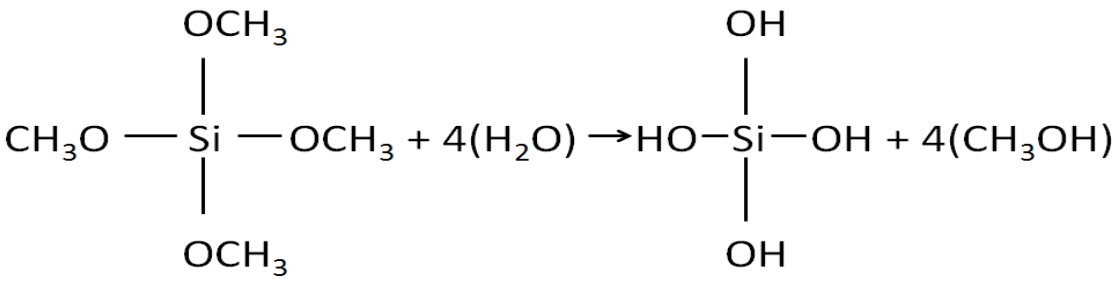

By definition, condensation liberates a small molecule, such as water or alcohol. This type of reaction can continue to build larger and larger silicon-containing molecules by the process of polymerization [24]. A condensation can occur between a silanol and an ethoxy group to form a bridging oxygen or siloxane group Si-O-Si [25].

Condensation

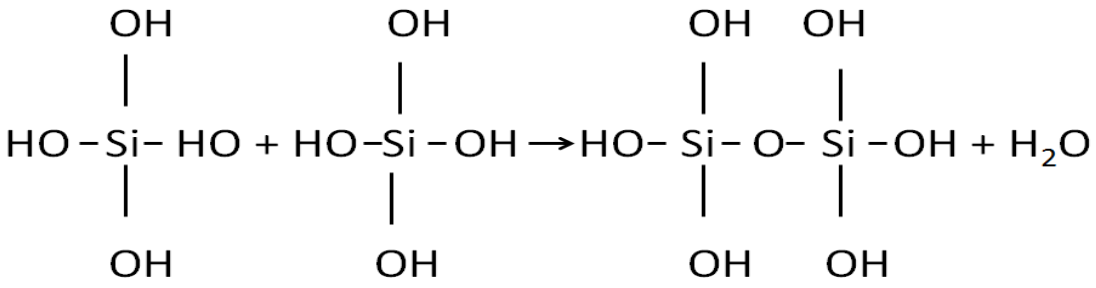

The H_2O (in condensation) and alcohol (in hydrolysis) expelled from the reaction remains in the pores of the network as shown in the following equation:

Polycondensation

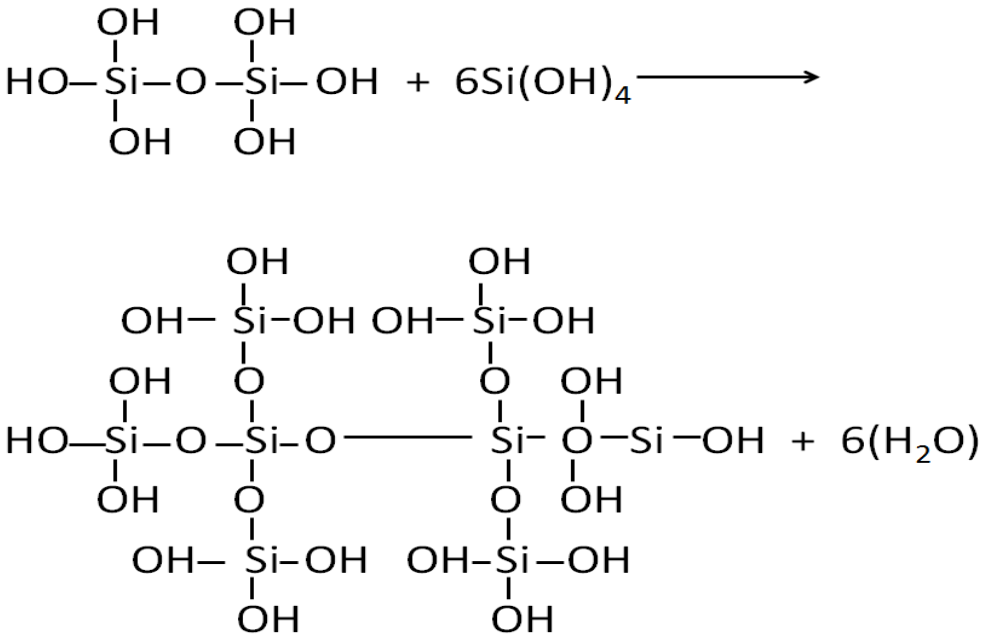

Figure 2.3: Synthesis reaction for the formation of each Si-O-Si

The phase establishes a 3D network that invades the whole volume of the container and as the reaction progresses, each side of the tetrahedral formed around silica becomes connected through oxygen to another silicon atom and forms a three dimensional network. This network is best described as possessing an order as described for an amorphous glass [26]. Thus a gel is obtained and for these two syntheses the liquid used as a solvent to perform the different chemical reaction remains within the pores of the solid network and once the sol reactions are complete, temperature dependent gelation, aging and drying processes take over. To increase the density of the material and remove the by-products, we must follow the sol-gel synthesis process by a high annealing schedule.

2.4.1 Gelation and Aging

As the hydrolysis and condensation polymerization reactions continue, viscosity increases until the solution ceases to flow. The time required for gelation to occur is an important

characteristic that is sensitive to the chemistry of the solution and the nature of the polymeric species. This sol-to-gel transition is nature is irreversible.

2.4.2 Drying

The drying phase involves the removal of the liquid phase; the gel transforms from an alcogel to a xerogel. Low temperature evaporation is frequently employed, and there is considerable weight loss and shrinkage. The drying stage is critical part of the so-gel process. As evaporation occurs, drying stresses arise that can cause catastrophic cracking of bulk materials. This effect is caused by evaporation of solvent molecules from the network of pores of the drying gels [19, 27].

2.4.3 Densification

This is the final step of the sol-gel process. At this point the gel-to-glass conversion occurs and the gel achieves the properties of the glass. As the temperature increases, several processes occur, including elimination of residual water and organic substances, relaxation of the gel structure, and ultimately, densification.

References

[1] S. Hussain, the Department of Physics, Chemistry and Biology, Linköpings University, (2008)

[2] J. K. Behera, Master of Science in Physics, National Institute of Technology, India

[3] Z. Liu, Z. Jin, W. Li, J. Qui, *Mat. Lett.* **59** 3620-3625 (2005)

[4] Ü. Özgür, Y. I. Alivov, C. Liu, A. Teke, M. A. Reshchikov, S. Doğan, V. Avrutin, S. J. Cho, and H. Morkoç, *Journ. Appl. Phys.* **98** 1-103 (2005)

[5] S. J. Pearton, D. P. Norton, K. Ip, Y.W. Heo, T. Steinerb, *Superlattices and Microstructures* **34** 29-32 (2003)

[6] J. Duan, H. Wang, X. Huang, *Chinese Journ. Chem. Phys.*, Volume 20, number 6, (2007)

[7] A. G. Ali, MSc Thesis, University of the Free State, Republic of South Africa, 2009

[8] R. S. Panwar, MSc Thesis, School of Physics and Materials science Thapar University, Patiala, (Punjab), 2009

[9] W. M. Hlaing OO, PhD dissertation, Washington State University, 2007

[10] http://en.wikipedia.org/wiki/Zinc_oxide [09 September 2011]

[11] E. Harrison, *Phys. Rev.* **93** 52-62 (1954)

[12] C. G. Van de Walle, *Physica B* **308-310** 899-903 (2001)

[13] http://www.lcc-toulouse.fr/lcc/IMG/pdf/optical_properties.pdf [21 September 2011]

[14] B. K. Meyer, H. Alves, D. M. Hofmann, W. Kriegseis, D. Forster, F. Bertram, J. Christen, A. Hoffmann, M. StraSSburg, M. Dworzak, U. Haboeck, A. V. Rodina, *Phys. Stat. Sol.* (b) **241** 231-260 (2004)

[15] P. Dahany, V. Fleurovy, P. Thurianz, R. Heitzz, A. Hoffmannz, and I. Broserz, J. *Phys. Condens. Matter.* **10** 2007-2019 (1998)

[16] http://www.psrc.usm.edu/mauritz/solgel.html [20 September 2011]

[17] L. F. Koao, MSc thesis, University of the Free State, Republic of South Africa, 2009

[18] mhtml:file://C:\Documents and Settings\uvp\My Document\Wiley *InterScience Jour…*

[19] http://sgmn.immt.pwr.wroc.pl/index.php?option=content&task=view&id=6&Itemid=30 [20 September 2011]

[20] http://encyclopedia2.thefreedictionary.com/Sol-gel+process [21 September 2011]

[21] http://gitam.edu/eresource/nano/NANOTECHNOLOGY/bottamup%20app.htm[19 September 2011]

[22] A. J. Silversmith, D. M. Boye, K. S. Brewer, C. E. Gillespie, Y. Lu and D. L. Campbell, *Journ. Lumin.* **121** 14-20 (2006)

[23] P. S. Mbule, MSc dissertation, University of the Free State, 2009

[24] http://en.wikipedia.org/wiki/Sol-gel [05 September 2011]

[25] L. C. Klein, *Annual Review of Materials Science*, **15** 227-248 (1985)

[26] G. F. Neilson, M. C. Weinberg, *J. Non-Cryst. Solids* **63** 365-374 (1984)

[27] http://what-when-how.com/materialsparts-and-finishes/sol-gel-process/ [22 September 2011]

CHAPTER 3

EXPERIMENTAL RESEARCH TECHNIQUES

3.1 Introduction

This chapter gives a description of the techniques that were used in the characterization of the ZnO nanostructures. These techniques includes the scanning electron microscopy (SEM), photoluminescence (PL), x-ray diffraction (XRD), UV-Vis spectroscopy, energy dispersive spectroscopy (EDS) and Fourier transform infrared spectroscopy (FTIR). SEM was used to obtain the morphology of the ZnO powders. PL and XRD were used to determine the crystalline size and shape of the compound formed and from the intensity peaks the particle size can be obtained. The UV-Vis was used to obtain the optical properties of the powders. EDS was used to monitor the elemental composition on the surfaces of ZnO powders.

3.2 Scanning electron microscopy (SEM)

The scanning electron microscope is designed for studying the surfaces of conducting and semi-conducting materials directly [1]. SEM is a type of electron microscope that images the sample surface by scanning it with a high energy beam of electrons in a raster scan pattern. SEM process begins with the electrons emitted from the electron gun. The electron beam that typically has an energy ranging from a few keV to 100 keV and is attracted to the anode, condensed and focused by a condenser lens and the objective lens into a beam with a very fine spot size. A beam of electrons is produced at the top of the microscope by an electron gun. The electron beam follows a vertical path through the microscope, which is held within a vacuum. The beam travels through electromagnetic fields and lenses, which focus the beam down toward the sample. Once the beam hits the sample, electrons and X-rays are ejected from the sample. Detectors collect these X-rays, backscattered electrons, and secondary electrons and convert them into a signal that is sent to a screen similar to a television screen. This produces the final image.

A simplified layout of a SEM is shown in ***Figure 3.1***, consisting of an electron gun, magnetic lens used to form the beam and limit the amount of current in the beam, and detectors. Electrons are produced via a thermionic emission from an electron gun and focused down to a spot on the specimen by a system of ion optics (i.e. electromagnetic coils). A set of scan coils are used to scan the spot over the surface of the sample and reflected electrons are collected, amplified and converted into a video signal.

The SEM is also responsible for obtaining the sample's surface topography, composition and other properties. This technique can give magnification to x300 000. The scanning electron microscope has many advantages over traditional microscopes. The SEM has a large depth of field, which allows more of a specimen to be in focus at one time. The SEM also has much higher resolution; closely spaced specimens can be magnified at much higher levels [2]. The SEM model which was used was a SHIMADZU SSX-550 SUPERSCAN SEM, seen in ***Figure 3.2***.

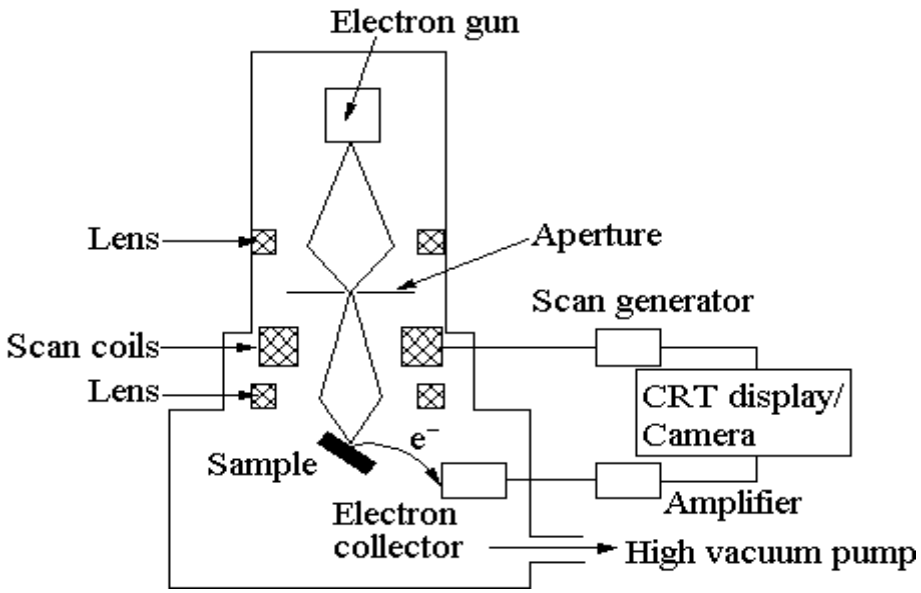

Figure 3.1: Schematic presentation of a Scanning Electron Microscopy [3].

Figure 3.2: SHIMADZU SSX-550 SUPERSCAN SEM with EDS.

3.3 Energy dispersive spectroscopy (EDS)

Energy dispersive X-ray spectroscopy is a relatively simple yet powerful technique used to identify the elemental composition of as little as a cubic micron of material. The equipment is attached to the SEM to allow for elemental information to be gathered about the specimen under investigation. EDS makes use of the X-ray spectrum emitted by a solid sample bombarded with a focused beam of electrons to obtain a localized chemical analysis. By scanning the beam in a television-like raster and displaying the intensity of a selected X-ray line, element distribution images can be produced. Also, images produced by electrons collected from the sample reveal surface topography or mean atomic number differences according to the mode selected. The scanning electron microscope (SEM), which is closely related to the electron probe is designed primarily for producing electron images, but can also be used for element mapping, and even point analysis, if an X-ray spectrometer is added. There is thus a considerable overlap in the functions of these instruments.

As a type of spectroscopy, it relies on the investigation of a sample through interactions between electromagnetic radiation and matter, analyzing X-rays emitted by the matter in response to being hit with charged particles. Its characterization capabilities are due in large part to the fundamental principle that each element has a unique atomic structure allowing x-rays that are characteristic of an element's atomic structure to be identified uniquely from each other. To stimulate the emission of characteristic X-rays from a specimen, a high energy beam of charged particles such as electrons or a beam of X-rays, is focused into the sample being studied.

There are four primary components of the EDS setup, the beam source, the x-ray detector, the pulse processor and analyzer. However, EDS systems are most commonly found on Scanning Electron Microscopes (SEM-EDS) and EDS used in this study is shown in ***Figure 3.2***. A detector is used to convert X-ray energy into voltage signals, this information is sent to a pulse processor, which measures the signals and passes them onto analyzer for data display and analysis.

3.4 Photoluminescence Spectroscopy (PL) (He-Cd Laser)

Photoluminescence is a process in which a substance absorbs photons (electromagnetic radiation) and then re-radiates photons. Quantum mechanically this can be described as an excitation to a higher energy state and then a return to a lower energy state accompanied by the emission of a photon [4]. The Helium-Cadmium (He-Cd) laser is one of a class of gas lasers using helium in conjunction with a metal which vaporizes at a relatively low temperature. A typical construction for the He-Cd laser is in the form of a tube, terminated by two Brewster's angle windows, with the two laser mirrors mounted separated from the tube. The tube filled with helium, also has a reservoir containing the Cd and a heater to vaporize the metal [5]. The reservoir is raised to a high enough temperature (~250 °C) to produce the desired vapour of Cd atoms in the tube. He-Cd laser can give output powers of 50-100 mW and it can produce a high quality beam at 442 nm (violet-blue) or 325 nm (UV) depending on the optics [5].

In a PL system the sample is excited with a monochromatized lamp or a higher laser beam, which is followed by the excitation during electron transition to higher energy levels and emission of photons during transition to the ground state [6].

The PL data was again collected using the Cary Eclipse Spectrophotometer (Figure 3.3 (b)). The Cary Eclipse Spectrophotometer uses a Xenon flash lamp (60-75 W) for superior sensitivity, high signal-to-noise, and fast kinetics. It measures the emission of light from samples in four modes. Using Xenon lamp technology, it captures a data point every 12.5 ms and scans at 24,000 nm/min without peak shifts. The Cary Eclipse is the only spectrophotometer with room light immunity.

Figure 3.3 (a): He-Cd (325 nm) laser used for photoluminescence.

Figure 3.3 (b): The Cary Eclipse Fluorescence Spectrophotometer at the University of the Free State, Physics department.

3.5 X-ray diffraction (XRD)

XRD is the science of determining the arrangement of atoms within a crystal from the manner in which a beam of X-rays is scattered from the electrons within the crystal. A crystal is a solid in which a particular arrangement of atoms (its unit cell) is repeated indefinitely along three principal directions known as the basis (or lattice) vectors. X-ray Diffraction is a powerful non-destructive technique used to investigate structural properties of crystalline materials [6]. Each crystalline solid has a unique XRD pattern to identify its crystal structure. When X-ray light with a wavelength λ is incident on a crystal, a diffraction peak occurs if the Bragg condition is satisfied:

$$n\lambda = 2d \sin\theta$$

where *n* is an integer 1, 2, 3….. (usually equal 1), d is the lattice spacing of the crystal and θ is the angle of incidence. The Cu K_α emission (λ = 1.5418 Å) from a copper target is the most common X-ray source for the diffraction measurement. Varying the angle θ, the

polycrystalline materials d-spacing are satisfied by the Bragg's Law conditions [6]. A powder XRD pattern is also used to determine the average size of the nanoparticles. The particle size can be calculated by using the Scherrer formula:

$$D = \frac{0.9\lambda}{\beta_{1/2} cos\theta}$$

where λ is the wavelength of the X-ray, and β is width (in radians) of the peak at 2θ and D is the diameter of the crystallites. Figure 3.4 (a) shows the simple schematic diagram of a path followed by x-ray from the tube to the detector. The measurements in this work were performed using the D8 Bruker Advanced AXS GmbH X-ray diffractometer at the University of the Free State as shown in figure 3.4(b).

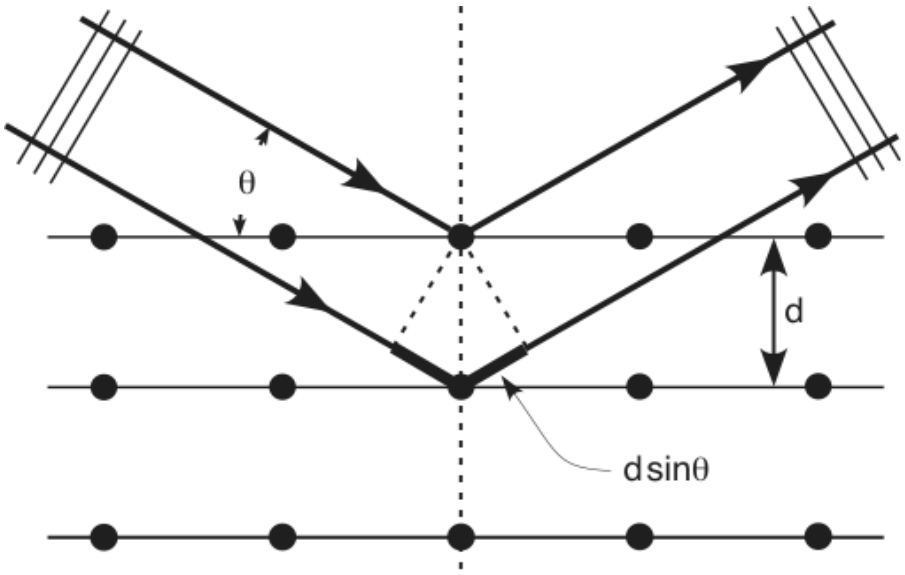

Figure 3.4 (a): Schematic diagram of diffractometer system.

Figure 3.4 (b): D8 Bruker Advanced AXS GmbH X-ray diffractometer.

3.6 Fourier Transform Infra Red (FTIR)

FT-IR stands for Fourier Transform Infra Red, the preferred method of infrared spectroscopy. In infrared spectroscopy, IR radiation is passed through a sample. Some of the infrared radiation is absorbed by the sample and some of it is passed through (transmitted). The resulting spectrum represents the molecular absorption and transmission, creating a molecular fingerprint of the sample. Like a fingerprint no two unique molecular structures produce the same infrared spectrum. This makes infrared spectroscopy useful for several types of analysis.

The process of how the FTIR works:

- **The Source:** Infrared energy is emitted from a glowing black-body source. This beam passes through an aperture which controls the amount of energy presented to the sample (and, ultimately, to the detector).

- **The Interferometer:** The beam enters the interferometer where the "spectral encoding" takes place. The resulting interferogram signal then exits the interferometer.
- **The Laser:** The Laser beam also passes through the interferometer. It is used for wavelength calibration, mirror position control and data collection triggering of the spectrometer
- **The Sample:** The beam enters the sample compartment where it is transmitted through or reflected off of the surface of the sample, depending on the type of analysis being accomplished. This is where specific frequencies of energy, which are uniquely characteristic of the sample, are absorbed.
- **The Detector:** The beam finally passes to the detector for final measurement. The detectors used are specially designed to measure the special interferogram signal.
- **The Computer:** The measured signal is digitized and sent to the computer where the Fourier transformation takes place. The final infrared spectrum is then presented to the user for interpretation and any further manipulation [8].

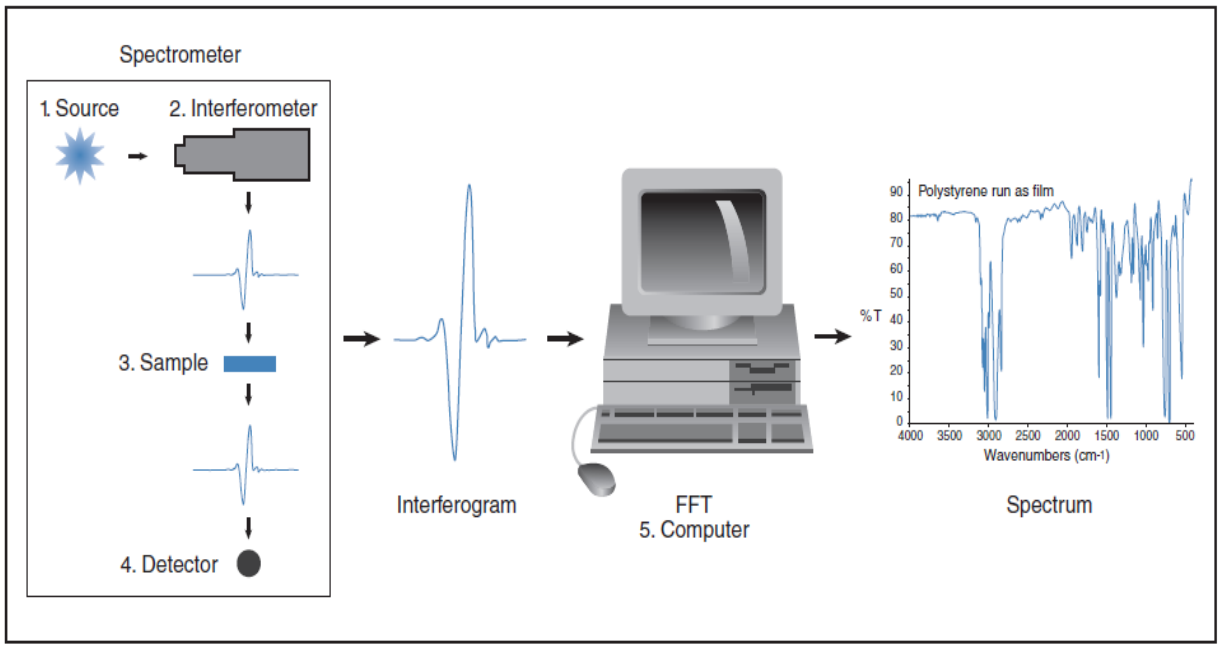

Figure 3.5(a): Schematic diagram of an FTIR [8].

Figure 3.5(b): Bruker TENSOR 27 Series FT-IR Spectrometer.

3.7 UV-Visible Spectrophotometer

An instrument used in the ultraviolet-visible spectroscopy is called UV/Vis spectrophotometer [9]. Fundamentally, the spectrophotometer (single beam) consists of the following elements: (1) a light source (usually a deuterium lamp for the UV spectral range and a tungsten lamp for the VIS and IR spectral ranges). Normally they are focused on the entrance to (2) a monochromator, which is used to select a single frequency wavelength from all those provided by the lamp source and scan over a desired frequency range, (3) a sample holder, followed by (4) a light detector (usually a photomultiplier for the UV-VIS range and a SPb cell for the IR range) to measure the intensity of each monochromatic beam after crossing the sample. Lastly, a computer registers the absorption spectrum [6].

Figure 3.6: Perkin Elmer Lamb 950 UV-VIS Spectrometer at the University of the Free Physics department.

References

[1] K. T. Hillie, Ph.D. thesis, University of the Free State, Republic of South Africa, October 2001, pp. 26

[2] Scanning Electron Microscope [online]. Available From http://www.purdue.edu/REM/rs/sem.htm 2008. [Accessed 8 August 2011]

[3]http://www.google.co.za/search?q=scanning+electron+microscopy&hl=en&prmd=imvnsb&tbm=isch&tbo=u&source=univ&sa=X&ei=1_BmT5C1L8PDhAeGiamxCA&ved=0CGMQsAQ&biw=1280&bih=929 [Accessed 28 February 2012]

[4] Photoluminescence [online]. http://en.wikipedia.org/wiki/Photoluminescence. [Accessed 24 August 2011]

[5] O. Svelto, Principles of lasers, 4th edition, *Springer, New York*, 1998

[6] P. A. Moleme, MSc thesis, University of the Free State, Republic of South Africa, 2011

[7] L. L. Yang, Linköping University, Linköping Studies in Science and Technology Licentiate Thesis No.1384, Sweden, 2008

[8] http://mmrc.caltech.edu/FTIR/FTIRintro.pdf [19 September 2011]

[9] P. S. Mbule, MSc thesis, University of the Free State, Republic of South Africa, 2009

CHAPTER 4

Synthesis and characterization of ZnO nanoparticles using Polyethylene Glycol (PEG)

4.1 Introduction

ZnO is an important material for room temperature UV lasers and short-wavelength optoelectronic devices [1]. Recently ZnO has attracted increasing interest due to its relatively high efficiency as a low-voltage phosphor [2]. ZnO is an oxide semiconductor known to have a wide band gap of about 3.2 eV for bulk materials and a large exciton binding energy of 60 meV, which enables efficient excitonic emission at room temperature [3]. ZnO is a compound that is reactive as an acid and as a base. It is almost insoluble in water and alcohol but it is soluble in acids. The optoelectronic properties of the material are sensitive to its crystal perfection and surface morphology. The photon emission efficiency decreases rapidly with the increase of non-radiative recombination centres. The crystalline quality of ZnO films is determined not only by the growth processes, but also by the dopants, impurities, surfactants and the surface modifiers such as polymer matrices used. Different methods such as hydrothermal [4] and solvothermal [5] methods have been used when preparing ZnO nanoparticles but in this investigation the sol-gel method was used and preferred for its advantages of being quick, inexpensive, reliable and simple. In general, the PL spectrum of ZnO consists of two bands, near band edge (NBE) excitonic UV emission and defect related deep level emission (DLE) around the green-yellow band extending from 2.9 eV to 1.65 eV, and this band almost covers the whole visible range of the electromagnetic (EM) spectrum **[6]**. The two carrier recombination routes compete with each other during the luminescence process. The improvement of NBE by post-growth annealing has been reported. However, the annealing conditions were different for the different researchers, and ranges from ambient

gas species, annealing temperature and annealing time [7-12]. It is also known that the location of the band-edge emission depends on the energy gap of the ZnO semiconductor [6]. In this study the effect of encapsulating ZnO nanoparticles with PEG on structural, morphological and optical properties were investigated. It is known that surface modification of nanoparticles by grafting polymers onto it is an effective way of improve its dispersability in a polymer matrix as well, and hence ameliorate the polymer matrix, thus enhancing the properties of the resulting composites [13].

4.2 Experimental procedure

PEG encapsulated ZnO nanoparticles were prepared with Zinc acetate dehydrate [$Zn(CH_3COOH)_2.2H_2O$] as a precursor in this experiment. This was done using the sol-gel method, 5.508g of $Zn(CH_3COOH)_2.2H_2O$ and various masses of PEG (0.5, 0.75, 1.0, 1.5, 2.0, and 2.5 g) were dissolved in 300 ml of ethanol with a ratio of 10:1 (Zn:PEG). This solution was magnetically stirred for 24 hrs at a temperature of 80°C until a clear solution was obtained. The resulting solution was left until a gel from this solution was obtained. The gel was then cleaned three to four times using methanol. After washing, it was calcined in the furnace in air at the temperature of 150°C for 2 hrs. These powders have been characterized under different techniques such as X-ray diffraction (XRD), Photoluminescence (PL), Scanning electron microscopy (SEM) and Energy dispersive spectroscopy (EDS). The influence of different molar masses of the PEG during the synthesis on the ZnO emission peaks was monitored.

4.3 Results and Discussion

4.3.1 Morphology and structure

A representative SEM image of ZnO and 1.0g PEG encapsulated ZnO are presented in Figure 4.1. The presence of agglomerated ZnO particles or some bigger particles for ZnO in Figure 4.1(a) could be attributed to the aggregating or overlapping of smaller particles. However, smaller monodispersed particles (see Figure 4.1(b)) are clearly visible for the PEG encapsulated ZnO particles. Therefore it is concluded that the presence of PEG has a significant influence on the structure and morphology of the ZnO. Figure 4.2 present typical XRD patterns of (a) ZnO and (b) PEG encapsulated ZnO nanostructures grown using sol-gel process, respectively. They both exhibit sharp diffraction peaks characteristic of the ZnO

wurtzite hexagonal phase (wurtzite-type, space group P63mc, JCPDS card file No. 36-1451), which implies that pure ZnO was formed. No characteristic diffraction peaks from other phases or impurities were detected. It was observed that by encapsulating the ZnO with PEG, an enhancement of the (002) peak relative intensity occurs, indicating a preferential growth orientation along the c-axis (Figure 4.2(b)). The broadness of the diffraction peaks measured with the XRD spectra indicated that nanoparticles were obtained for both ZnO and the PEG encapsulated ZnO particles. The findings agree with the SEM micrographs of the samples showing that PEG encapsulated ZnO nanostructures are smaller in size. The chunks of material as seen on the pure ZnO SEM image must therefore be agglomerated nanoparticles.

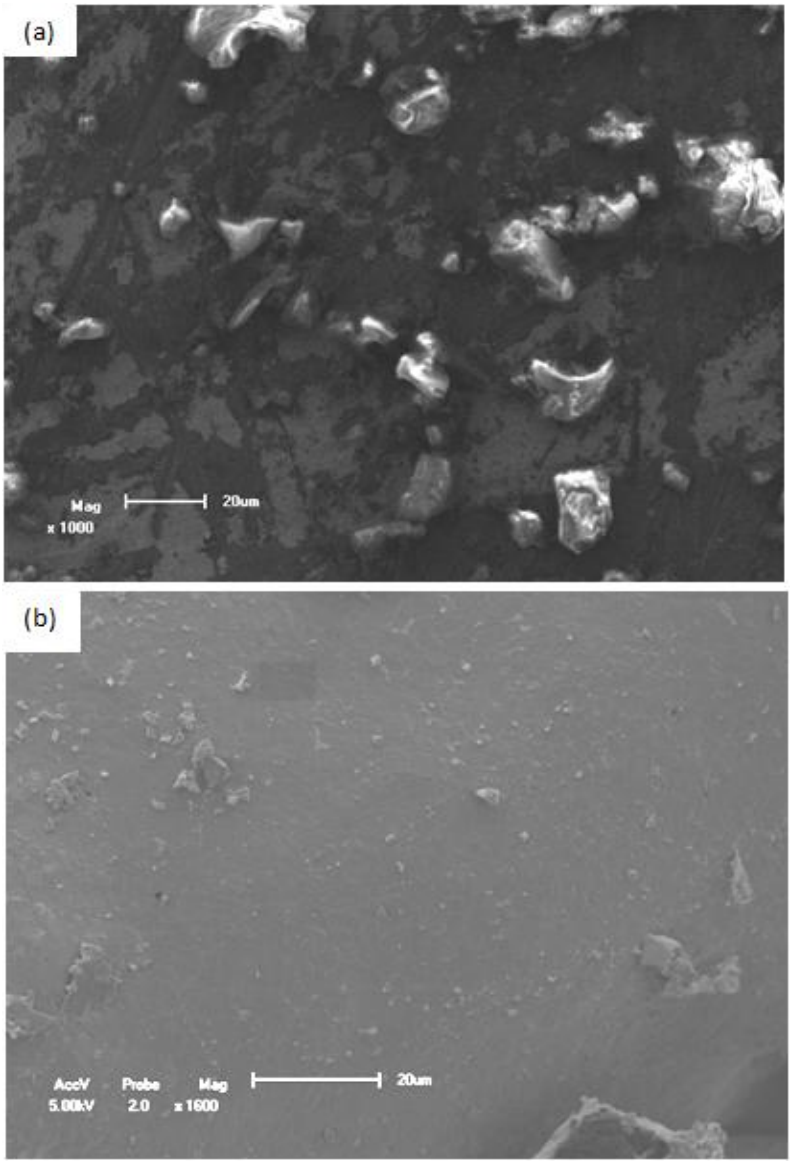

Figure 4.1(a): SEM image of the pure ZnO without any encapsulated PEG at x 1000 magnification (b) SEM image of the ZnO synthesized with 1.5g PEG at x 1600 magnification.

The particle size of the agglomerated particles were calculated by using the full width at half maximum (FWHM) value of the of the (002) diffraction peak for the 1.0g PEG encapsulated ZnO and ZnO samples, using the Debye-Scherrer formula;

$$D = \frac{0.9\lambda}{\beta_{1/2} cos\theta}$$

Where λ is the wavelength (1.5406 Å), D is the diameter of the crystallites, $\beta_{1/2}$ is the full-width at a half-maximum (FWHM) and θ is the diffraction angle. The capsulated particle sizes of ZnO and PEG encapsulated ZnO were found to be 43 nm and 28 nm respectively. The wurtzite lattice parameters a and c calculated from XRD spectra are (a = 3.25Å, c = 5.20Å), (a = 3.24Å, c = 5.19Å) for ZnO and the PEG encapsulated ZnO nanoparticles samples. These parameters were calculated using the planes (102), (110), (103) and (200) [14]. The volume of the unit cell for the ZnO and PEG encapsulated ZnO nanoparticles are 54.9$Å^3$ and 54.5$Å^3$.

4.3.2 Optical properties

The optical absorption of the ZnO in this case is observed with the UV-Visible near infrared spectrometer. The prepared nanopowders were first dispersed in ethanol and then the UV-VIS optical absorption characteristics of the ZnO nanoparticles were measured. The measured absorption characteristics of the ZnO prepared with different molar masses of the polymer PEG are shown in Figure 4.3. The synthesis of the ZnO nanoparticles is clearly evident from Figure 4.3. A big jump which is observed on the absorbance intensity is due to the impact that the encapsulation of PEG has brought on the particles. Each sample brings about change on the absorbance intensity. It is observed that absorption of ZnO is very sharp, which indicates the monodispersed nature of the nanoparticle distribution [7-9]. The absorption edge for single crystal ZnO is very sharp and is determined by the nature of the electronic transition between the valence band and conduction band. The absorption edge for a suspension of nanoparticles is much broader and is determined by the distribution of particle size [11]. At the absorption edge, only the largest particles contribute to the absorbance. In the smaller wavelength range particles with smaller sizes contribute more and at the region of maximum absorbance, all particles contribute to the absorbance. Thus the average particle size present in a nanocolloid can be determined from the inflection point in the absorption vs. wavelength spectrum [11]. From this figure it is seen that the band edge

appearing between 360 nm and 380 nm shows a blue shift with an increase in some of the molar masses of PEG. This might be due to that the PEG has taken over the surface of the ZnO nanoparticles.

Photoluminescence (PL) of PEG encapsulated ZnO nanoparticles studied in comparison with ZnO nanopowder using a 325 nm He-Cd (26mW) laser with excitation frequency 325nm at room temperature are shown in Figure 4.4(a). Two prominent emissions peaks one green at around 560 nm and another blue at around 450 nm without near band-edge (NBE) ultraviolet (UV) peak were observed. It is generally accepted that the surface states play a crucial role in the PL spectra of nanomaterials [15]. The green peak of ZnO is due to radiative recombination of a photo-generated hole with an electron attributed to an oxygen vacancy [15]. The amount of oxygen in the surface is expected to drastically change the green-band peak. The presence of PEG on the surface has a controlling effect on the concentration of surface oxygen vacancies. Different concentrations of PEG have brought an impact on the intensity of both the blue and the green peaks, the blue peaks shows a high intensity meaning smaller particles were obtained (see Figure 4.4(b)). Except for a clear shift in the peak position from the ZnO nanoparticles to the ZnO particles encapsulated in the PEG, there is no definite trend in peak intensity as function of PEG molar mass measured. At this point it is therefore difficult to pinpoint an exact mechanism due to the lack of detailed information about surface band bending and related surface species of ZnO [16, 17 and 18]. Important however is that it is evident from the results that the UV peak emission is suppressed. The amount of the PEG masses applied seems to have significant effects on the enhancement of both the blue and green emissions without a proportional relation. The PEG masses of 0.5, 0.75 and 2.0 g significantly enhanced the blue emission while PEG masses of 1, 1.5 and 2.5 g produces emission of approximately equivalent intensity. It is therefore clear that the PEG played a role in the suppressing and enhancement of maximum intensity as well as in the peak shape of the obtained emission spectra. Further studies are needed to clearly understand the total effect of the different PEG concentrations.

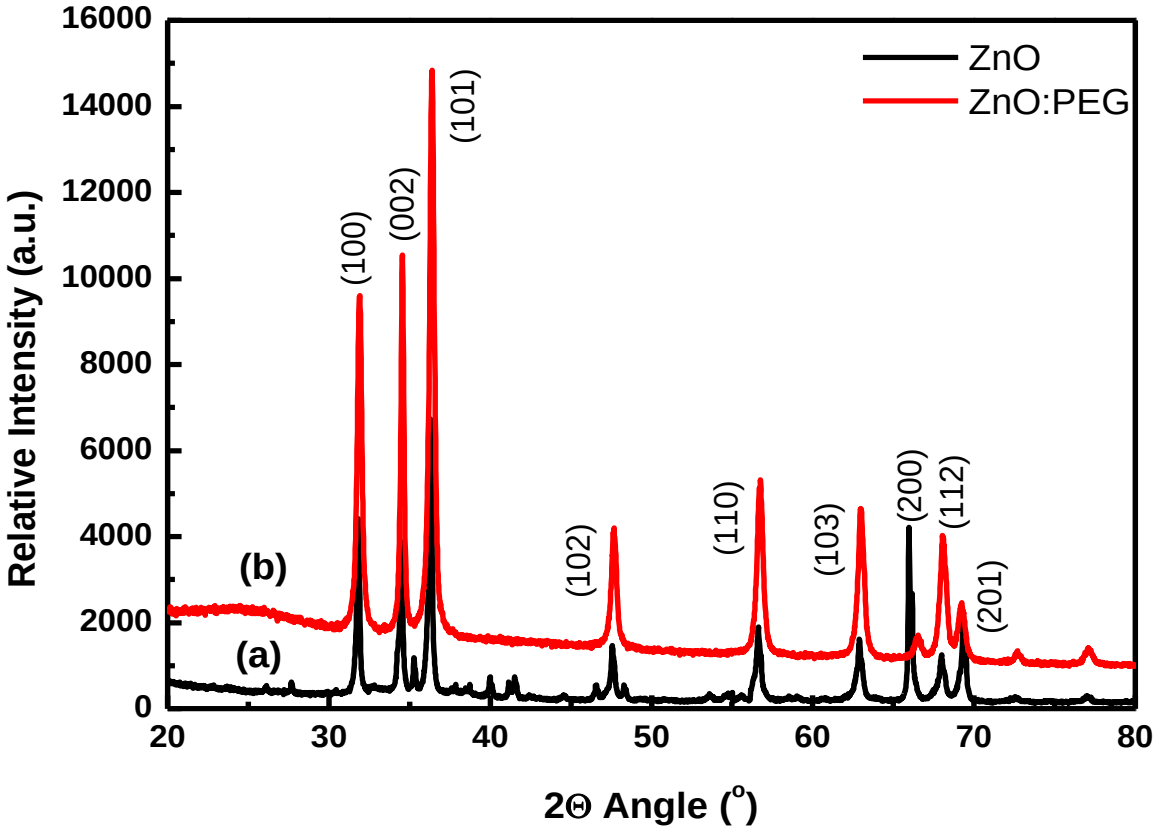

Figure 4.2: XRD spectra of the ZnO synthesized with 1.5 g.

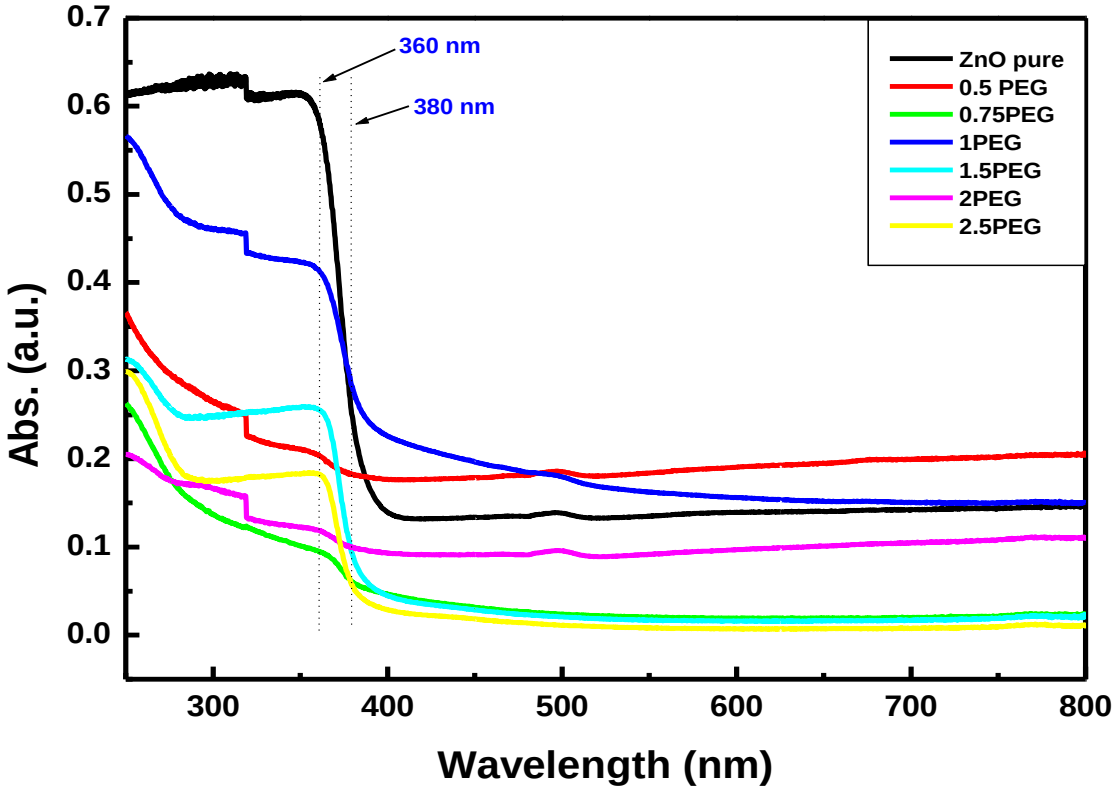

Figure 4.3: UV-Visible absorbance spectra of the ZnO synthesized with different molar masses of PEG.

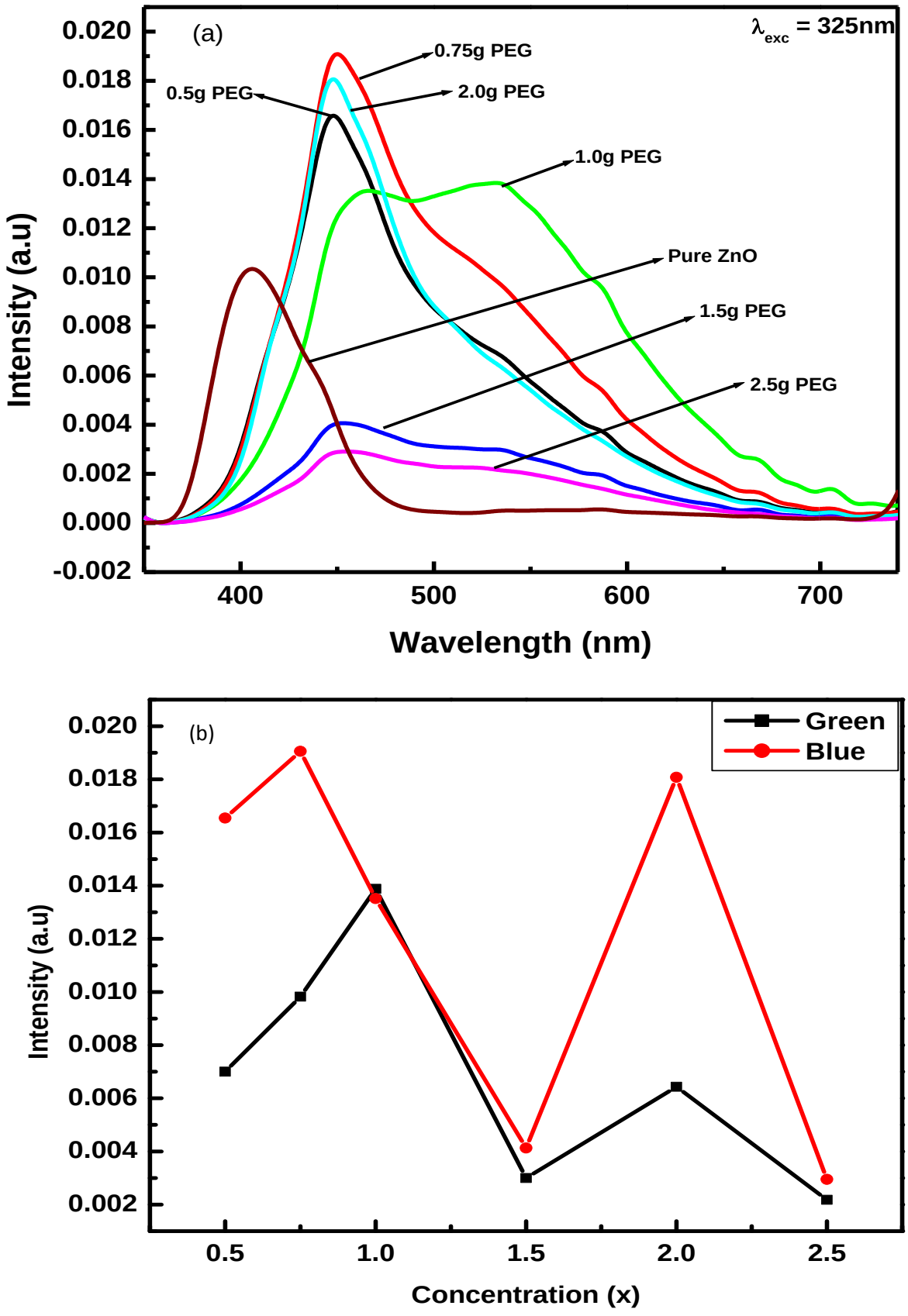

Figure 4.4: (a) PL emission spectra of the ZnO prepared with different molar masses of PEG (b) PL emission intensity versus concentrations of PEG encapsulated ZnO nanoparticles.

4.4 Conclusion

In this work, we successfully synthesized monodispersed ZnO nanoparticles with average size of 20 nm by a chemical method by PEG as capping agent and alcohol as solvent. The nanostructures of the prepared ZnO nanoparticles have been confirmed using UV-VIS absorption, XRD, and SEM micrograph analysis. The PL emissions from the ZnO nanoparticles dispersed in ethanol have been measured under 325 nm UV light excitations. The maximum PL emission has been observed covering the 400-700 nm visible region of the electromagnetic spectrum, when a 325 nm wavelength is used for excitation. The strong blue and green luminescence observed, demonstrates the good quality of the prepared ZnO nanoparticles. As suggested and confirmed by others [19, 20] that such low energy emissions are assigned to the surface states. The density of surface states in the nanocrystals would increase with a decrease in the size of crystallites of the prepared nanocrystals, due to the increased surface-to-volume ratio having smaller crystallites. This would reduce the probability of excitonic emission via non-radiative surface recombination [19, 20].

References

[1] S. Suwanboon, *Science Asia* **34**, 031-034 (2008)

[2] Y. L. Zhang, Y. Yang, J. H. Zhao, R.Q. Tan, P. Cui, W.J. Song, *J. Sol-Gel Sci. Technol*, **51** 198-203 (2009)

[3] D. C. Look, *Mater. Sci. Eng. B* **75** 190 (2000)

[4] D. Yiamsawas, K. Boonpavanitchakul, and W. Kangwansupamonkon, *Journ. Microscopy Society of Thailand*, **23** 75-78 (2009)

[5] L. Fan, H. Song, Te Li, L. Yu, Z. Liu, G. Pan, Y. Lei, X. Bai, T. Wang, Z. Zheng, X. Kong, *J. of Lumin*. **122–123** 819-821 (2007)

[6] H. Mao, K. Yu, J. Wang, J. Yu, and Z. Zhu, *Optics Express* **17** 11861 (2009)

[7] K. Vanheusden, W. L. Warren, C. H. Seager, D. R. Tallant, J. A. Voigt, B. E. Gnade, *Appl. Phys*. **79** 7983-7990 (1996)

[8] W. S. Shi, O. Agyeman, C.N. Xu, *J. Appl. Phys*. **91** 5640-5644 (2002)

[9] K. Ogata, K. Sakurai, S. Fujita, S. Fujita, K. Matsushige, *J. Crystal Growth* **214/215** 312-315 (2000)

[10] J. Cho, J. Nah, M. S. Oh, J. H. Song, K. H. Yoon, H. J. Jung, W. K. Choi, *Jpn. J. Appl. Phys*. **40** L1040-L1043 (2001)

[11] K. Ozaki, M. Gomi, *Jpn. J. Appl. Phys*. **41** 5614-5617 (2002)

[12] N. Ohashi, T. Ishigaki, N. Okada, T. Sekiguchi, I. Sakaguchi, H. Haneda, *Appl. Phys. Lett.* **80** 2869-2871 (2002)

[13] A. Matei, I. Cernica, O. Cadar, C. Roman, V. Schiopu, *Int. J. Mater FormSuppl* 1:767-770, DOI 10.1007/s 12289-008-0288-5 (2008)

[14] B. D. Cullity, Addison Wesley, *2nd Ed*. 335-336 (1978, 1956)

[15] K. Vanheusden, C. H. Seager, W. L. Warren, D. R. Tallant, and J. A. Voigt, *Appl. Phys. Lett.* **68** 403-405 (1996)

[16] B. J. Coppa, C. C. Fulton, S. M. Kiesel, R. F. Davis, C. Pandarinath, J. E. Burnette, R. J. Nemanich, D. J. Smith, *J. Appl. Phys*. **97**, 103517-1 – 103517-13 (2005)

[17] S. A. Chevtchenko, J. C. Moore, U. Ozgur, X. Gu, A. A. Baski, H. Morkoc, B. Nemeth, J.E. Nause, *Appl. Phys. Lett*. **89**, 182111-1 – 182111-3 (2006)

[18] S. J. Cho, S. Dogan, S. Sabuktagin, M. A. Reshchikov, D. K. Johnstone, H. Morkoc, *Appl. Phys. Lett.* **84** 3070-3072 (2004)

[19] M. Vafaee and M. S. Ghamsari, *Mat. Lett.* **61** 3265-3268 (2007)

[20] M. Wang, E. K. Na, J. S. Kim, E. J. Kim, S. H. Hahn, C. Park, and K. Koo, *Materials Lett.* **61** 4094-4096 (2007)

CHAPTER 5

Synthesis and characterization of the ZnO nanoparticles and the polyvinyl pyrrolidone (PVP) encapsulated ZnO nanoparticles

5.1 Introduction

As a semiconductor material, zinc oxide spans a wide range of applications from solar cells and chemical sensors to electrical, acoustic and luminescent devices [1]. ZnO is also a versatile direct-band gap semiconductor with a wide band gap of 3.37 eV, and its large exciton binding energy (60 meV) makes the exciton state stable even at room temperature. Furthermore, it is an environmentally friendly material and shows a broad luminescence emission spectrum in the blue-yellow region [2]. ZnO appears to be a major candidate for room temperature optoelectronic applications such as efficient short-wavelength ultraviolet light-emitting diodes and laser diodes [3]. Various processes have been employed to synthesize the ZnO nanostructures, such as electrochemical deposition [4], hydrothermal [5], sputter deposition technique [6], and vapour method [7]. From all these methods, we have chosen to use the sol-gel method because of its reliability, inexpensiveness and most of all simplicity. The crystalline quality of ZnO films is determined not only by the growth processes, but also by the do-pants, impurities, surfactants and the surface modifiers such as polymer matrices used. The nanoparticles which are produced by this route show good optical properties, but this can be achieved only by good control of the size and the morphology of the particles [8]. Several workers have used capping agents such as poly vinyl pyridine (PVP), poly ethylene glycol (PEG) etc to stop particle agglomeration and obtained nanoparticles of size less than 5 nm and these polymers produce spherical nanoparticles in shape because of the property of surface tension [9]. PVP is utilized to make ZnO nanorods from a zinc acetate precursor at a low temperature, since the PVP can easily be removed by burning the solid products [10]. In this investigation we concentrating on the encapsulated

ZnO nanoparticles and the effect that PVP have on the optical properties and the morphology and structure of the ZnO powders.

5.2 Experimental

The solutions of ZnO were prepared by dissolving 5.508 g of Zinc Acetate in 300 mL of ethanol with different masses of PVP. This was repeated six times with the following different molar masses; 0.5, 0.75, 1.0, 1.5, 2.0 and 2.5g. The mixtures were magnetically stirred for about 24 hours at a temperature of 80°C; this was to let the mixture mix thoroughly. The mixtures where let on the stirrer until the gel-like of the zinc acetate and PVP was obtained. It was then washed using methanol to remove the impurities. Then the gel was calcined in a furnace at 150 °C for 2 hours. The X-ray diffraction (XRD) patterns were recorded to characterize the phase and crystal structure of the nanoparticles using a D8 Bruker Advanced AXS GmbH X-ray diffractometer (XRD), room temperature photoluminescence (PL) of the samples was measured, using a He–Cd laser (325 nm) as excitation sources, the morphology of the nanoparticles was observed by a Shimadzu Superscan SSX-550 system scanning electron microscope (SEM) operated at 20 kV equipped with energy dispersive X-ray spectroscopy (EDS). Optical absorption was performed on a Perkin Elmer Lamb 950 UV-visible spectrophotometer (UV).

5.3 Results and Discussion

5.3.1 Structure

In this part, we studied the role of PVP molar masses in controlling the size and shape of the PVP encapsulated ZnO nanoparticles. Figure 5.1(a) represents the SEM image of the PVP encapsulated ZnO nanoparticles. The figure shows the chunk of particles which probably consist out of agglomerated smaller particles in the PVP matrix; the agglomeration is due to the aggregating or overlapping of smaller particles. However, small agglomerates on some of the large particles are clearly visible at high magnifications. Therefore it is concluded that the chosen PVP/Zn^{2+} molar ratio range has influence on the morphology of the ZnO samples. Figure 5.1(b) is the EDS for the encapsulated ZnO nanoparticles. It gives out the elements that exist in the sample. All expected elements (Zn, O) were detected and the adventitious carbon is also to be seen. Figure 5.2 (a) and (b) are the powder x-ray diffraction pattern (XRD) of the ZnO nanoparticles and the 0.5 g PVP encapsulated ZnO nanoparticles. The

ZnO nanoparticles pattern showed the standard diffraction pattern of wurtzite hexagonal ZnO. Figure 5.2(b) shows that the XRD peak positions shifted as well as the peaks have broadened. This confirms that the PVP has an effect on the structure of the ZnO nanoparticles. The crystallite size was calculated from the peaks width using the Debye-Scherer formula

$$D = \frac{0.9\lambda}{\beta_{1/2} cos\theta}$$

Where λ is the x-ray wavelength (1.5406Å), θ is the Bragg diffraction angle, D is the diameter of the crystallites, and β is the peak width at half maximum (FWHM). The particle sizes of the encapsulated PVP ZnO and ZnO nanoparticles were calculated were found to be 13 nm and 42 nm. The XRD peaks in Figure 5.2(a) gave lattice parameters a = 3.25 Å and c = 5.20 Å and that of Figure 5.2(b) are a = 3.25 Å and c = 4.88 Å.

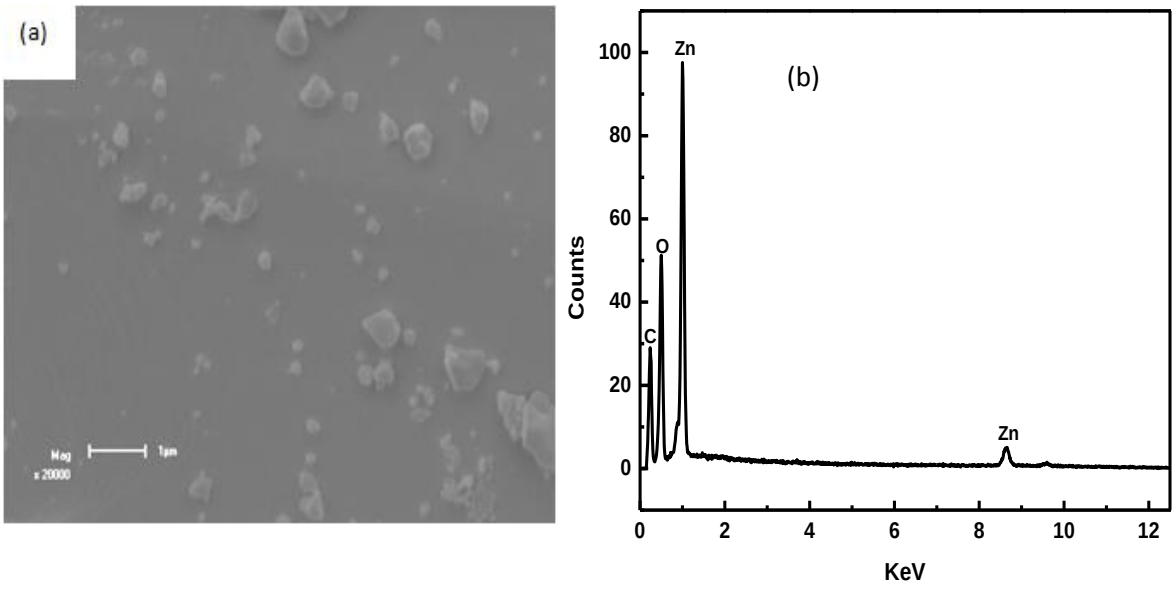

Figure 5.1: (a) SEM image of the ZnO (b) EDS spectra for the ZnO nanoparticles capsulated in PVP which confirms the presence of the different elements.

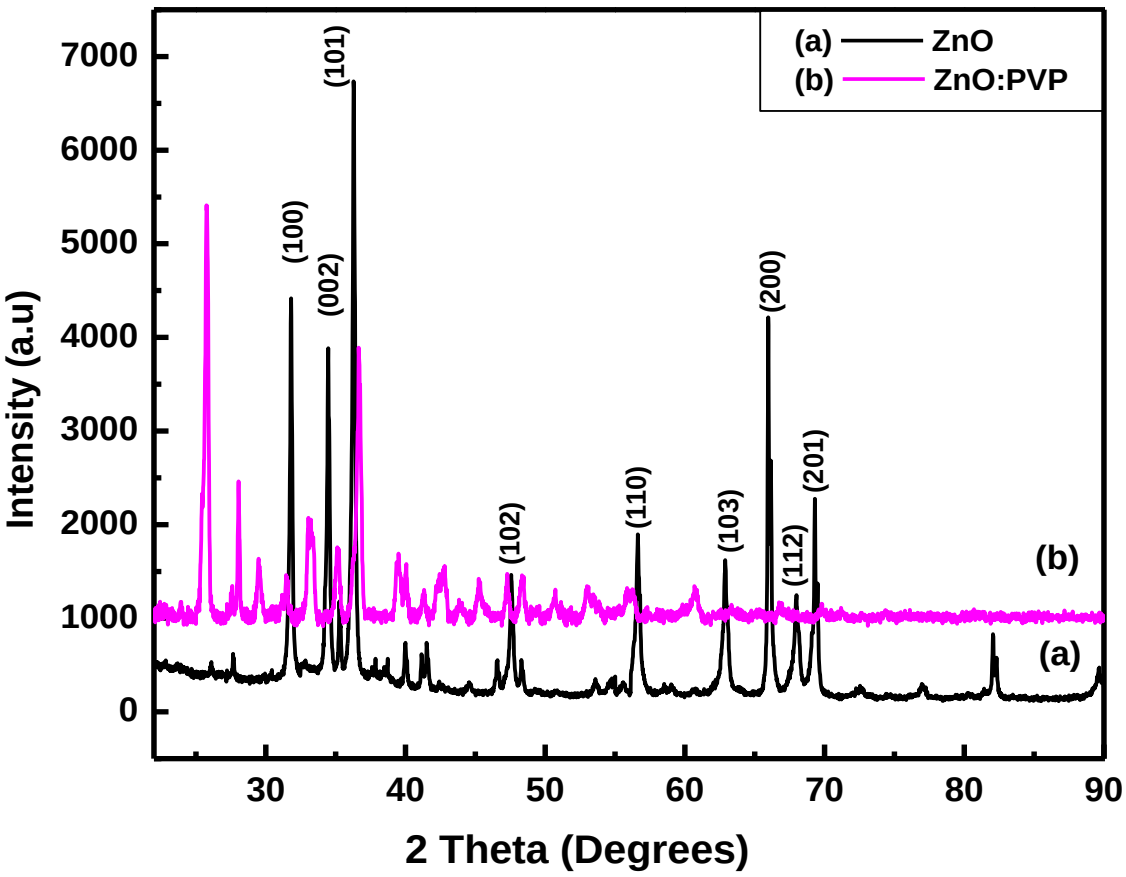

Figure 5.2: XRD patterns of (a) ZnO nanoparticles and (b) PVP encapsulated ZnO nanoparticles.

5.3.2 Optical properties

The photoluminescence spectra of the seven different concentrations of PVP samples, which were recorded with the excitation wavelength set at 325 nm, as shown in Figure 5.3. The two emission peaks, one a blue emission peak around 448 nm and another green emission peak around 532 nm, were observed for all samples except for the sample with no PVP. The sample without PVP shows only one violet emission peak around 403 nm. Comparing the maximum intensity and peak shape of the six samples with the one without PVP, it is observed that PVP has a clear effect on the ZnO nanoparticles. The relative intensities of these two emission band vary drastically with the molar ratio of Zn:PVP. The addition of the PVP has brought an increase in the intensity with various molar masses.

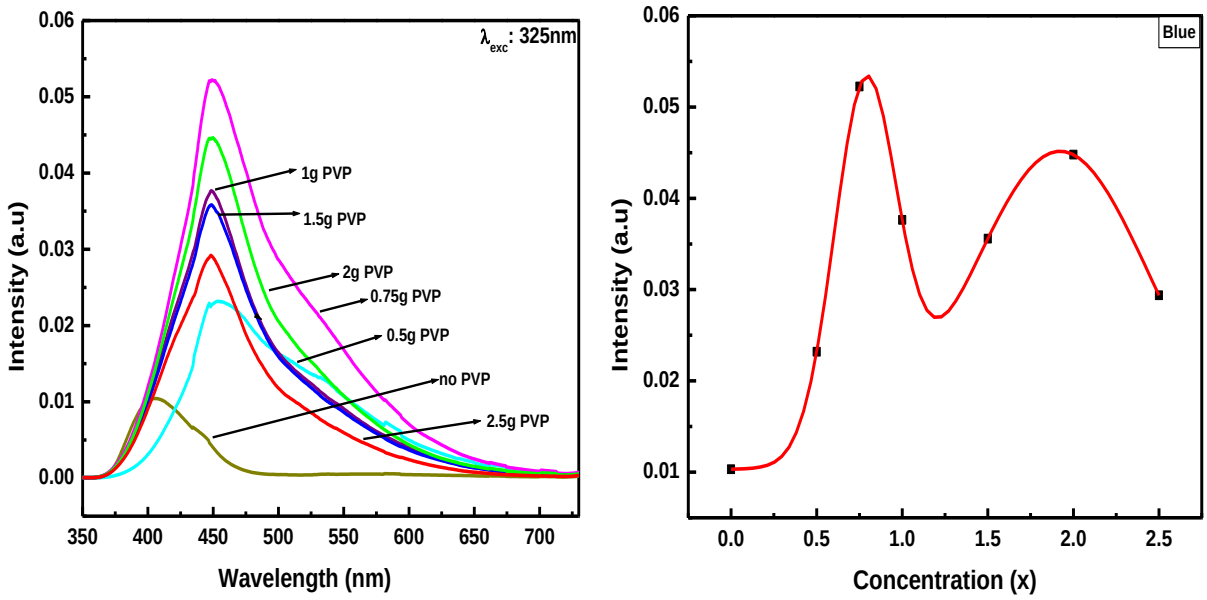

Figure 5.3: (a) PL emission spectra of the ZnO with different masses of PVP (b) PL emission intensity versus various masses of the PVP encapsulated ZnO nanoparticles.

Figure 5.3(b) shows the intensity versus the concentration or different masses of PVP which shows that the 0.75g of PVP has the highest intensity followed by the 2.0 g of PVP. The figure shows an increase on the intensity with an increase on the molar masses of PVP (0-0.75 g). A decrease on the intensity was observed for the molar mass 1.0 g and increased again as the molar masses increased. The absorption spectra of the PVP encapsulated ZnO nanoparticles with different masses of PVP are shown in Figure 5.4. The absorption peaks of PVP encapsulated ZnO are obtained at the wavelength of 272 nm and the other one at around 358 nm. The absorption peak at around 358 nm is a blue shift relative to the bulk exciton absorption (375 nm) [11], the shift might be due to the strong confinement effect [12]. There is a fluctuation of absorption peaks in addition of molar masses of PVP. The absorption peak at around 272 nm corresponds to the electron-hole conjunctions.

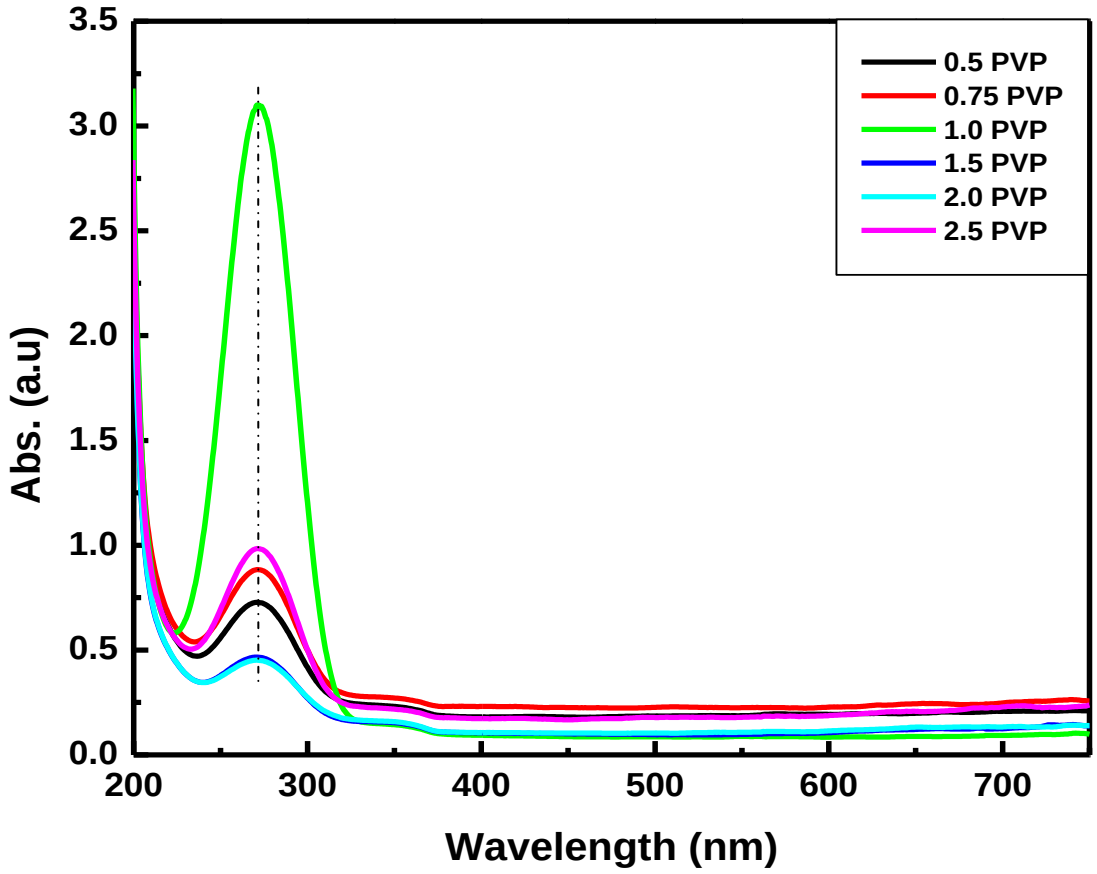

Figure 5.4: UV-visible absorbance various spectra of the PVP encapsulated ZnO nanoparticles.

5.4 Conclusion

In this investigation, the synthesis of PVP encapsulated ZnO nanoparticles with different molar mass of PVP was reported. This was done with the sol-gel method. The characterization was done using XRD, SEM, PL, and UV-VIS absorption. The PL covered the wavelength range of 350-750nm.

References

[1] C. Yang, Y. Ping, W. Jiannong, G. Weikun, and Wong G. K. L., *Chem. Mater.*, 12 (2000) 2268-2274

[2] Y. Yang, Y. Li, S. Fu, and H. Xiao, *J. Phys. Chem. C*, **112** (2008), 10553-10558

[3] G. Kenanakis, M. Androulidaki, E. Koudoumas, C. Savvakis, N. Katsarakis, *Superlattices and Microstructures* **42**, (2007) 473-478

[4] G. R. Li, D. L. Qu, W. X. Zhao, Y. X. Tong, *J. Mater. Chem.* **9**, (2007) 1661

[5] K. H. Tam, et al., *J. Phys. Chem.* B **110**, (2006) 20865

[6] W. T. Chiou, W. Y. Wu, J. M. Ting, *Diamond Relat. Mater.* **12** (2003)1841

[7] Y. Zhang, K. Yu, D. Jiang, Z. Zhu, H. Geng, L. Luo, *Appl. Surf. Sci.* **242** (2005) 212

[8] M. Vafaee, G. M. Sasani, *Materials Letters* **61**, (2007) 3265 – 3268

[9] G. Atul, H. S. Bhatti, D. Kumar, N. K. Verma, R. P. Tandon, *Digest Journal of Nanomaterials and Biostructures* Vol. **1**, No. 1, (2006), p.1- 9

[10] M. Eskandari, V. Ahmadi, S. H. Ahmadi, *Physica B* **404** (2009) 1924-1928

[11] J. Liu, X. Huang, Y. Li, J. Duan, H. Ai, L. Ren, *Materials Science and Engineering* B **127**, (2006), 85-90

[12] C. Yang, P. Yu, J. Wang, W. Ge, G. K. L. Wong, L. Guo, S. Yang, *Applied Physics Letters*, Volume 76, No. 20, (2000), 2901-2903

CHAPTER 6

Effects of the temperature on the ZnO properties by using various solvents

6.1 Introduction

Nanostructured ZnO semiconductor has drawn enormous attention due to its unique properties in optics, photonics and electronics [1]. Synthesizing the ZnO quantum particles using precipitation from alcohols results in stable colloids of nanometer-sized particles [2-4]. The powders were prepared using the sol-gel method. The influence of the solvent provides a means to achieve control over the ZnO nanoparticle size and size distribution, which is essential for tailoring optical, electrical, chemical, and magnetic properties of nanoparticles for specific applications [5]. The solvents also provides a means of temperature control, either to increase the energy of the colliding particles so that they will react more quickly, or to absorb heat that is generated during and exothermic reaction. The effect of solvents (organic) are reported by Zhang et al. [6] and Kwon et al. [7], concluded that solvents not only controls the morphology, but it also plays a vital role on the optoelectronic and electrical properties of nanosized ZnO. Water is a dipolar, amphiproitc solvent with a high dielectric constant and, as a consequence, most salts are readily dissolved where most alcohols are dipolar, amphiprotic solvents with a dielectric constant and viscosity that is dependent on the chain length [5]. The zinc cation is soluble in water and growth is controlled by the diffusion of Zn^{2+} ions in the ethanol-rich layer [8]. In this report nanostructure ZnO particles were prepared by adding NaOH into the solution of $Zn(CH_3COO)_2$ in ethanol, methanol and water. The aim of this work was to compare and contrast the dependence of material properties of ZnO nanostructures on the different solvents.

6.2 Experimental

ZnO nanoparticles were prepared by dissolving 4.3898 g of zinc acetate [$Zn(CH_3COO)_2.2H_2O$] in 100 ml of methanol, water or ethanol (0.2 M) using vigorous stirring

until the homogeneous solution was obtained. Then 3.2 g of NaOH was dissolved in 130 ml of ethanol (0.8 M), methanol or water in an ultrasonic bath and was also cooled in ice water. This solution was slowly added to the transparent Zn-solution using vigorous stirring at ambient temperature for 1 hour before filtering. The unwanted CH_3COO^- and Na^+ ions were removed by washing the precipitate repeatedly with deionised water. After filtering, the precipitate was then dried at 60°C for an hour and then annealed in air at 600 °C, 500 °C, 400 °C and 300 °C for 1 hour.

6.3 Results and discussion

6.3.1 Structural and morphology

Represented in the Figures 6.1 are the SEM images of the ZnO prepared using ethanol, methanol, or water as solvents. ZnO prepared with ethanol shows the ZnO nanostructures in a form of clustered nanorods which were calcined at a temperature of 300 °C whereas at a temperature of 600 °C the monodispersed ZnO particles. From these two SEM images, it is clearly seen that the morphology of the materials was affected by the temperature, which concludes that the temperature has an impact on the morphology of the ZnO.

SEM images of ZnO prepared using methanol presents the agglomerated ZnO nanoparticles resulting from overlapping of small particles when calcined at 300 °C and 600 °C. The annealing temperature seems to have an impact on the particle growth and the surface. Comparing the 300 °C with the 600 °C, the surface roughness has changed and the growth of the agglomerated nanoparticles have grown. Methanol has a high saturation vapour pressure and it was utilised as a reaction media so the combination of the nucleus is not intense due to lower boiling point of the solvent which results in spherical particles of ZnO prepared using methanol.

Figures 6.1(e) and (f) also gives the ZnO clustered nanorods prepared using water. The sizes of the ZnO nanorods prepared using ethanol and those prepared using water are not the same. In water, the reaction disperses more homogeneously than in organic solvents and the growth of the crystal nucleus is subjected to less confinement in boiling droplet of solvent. This reveals the impact that the solvents have on the morphology of the ZnO nanorods. The temperature also played an important role on the surface of the ZnO.

X-ray diffraction was used to investigate the structure of ZnO powders. The x-ray diffraction patterns for the ZnO particles prepared using different solvents; ethanol, methanol or water annealed at various temperatures are shown in Figures 6.2 - 6.4. Three pronounced ZnO peaks, (100), (002), and (101) appear at 2θ = 36.68 °, 34.44 °, and 36.32 ° respectively on these figures. The figures are indexed as hexagonal wurtzite structure ZnO (JCPDS 36-1451).

The XRD pattern of the ZnO ethanol prepared presented peaks that are not on the standard spectrum. These peaks might be due to the impurities during the synthesis; this is shown at a temperature of 500 °C.

ZnO prepared using water revealed that the (102) peak intensity varies with an increase in the annealing temperature. The strong and narrow diffraction peaks at high annealing temperature indicate that the material has improved crystallinity and larger particle size.

The (002) plane in Figure 6.3 at a temperature of 400 °C has a higher intensity as compared to the JCPDS for the ZnO. There is an increase on the intensity with an increase on the annealing temperature for the ZnO prepared with methanol. The influence of the calcination temperature in diffractograms of x-ray diffraction of the samples can be observed in the variations of intensity and full-width to medium-height (FWHM) of the diffraction peaks of ZnO.

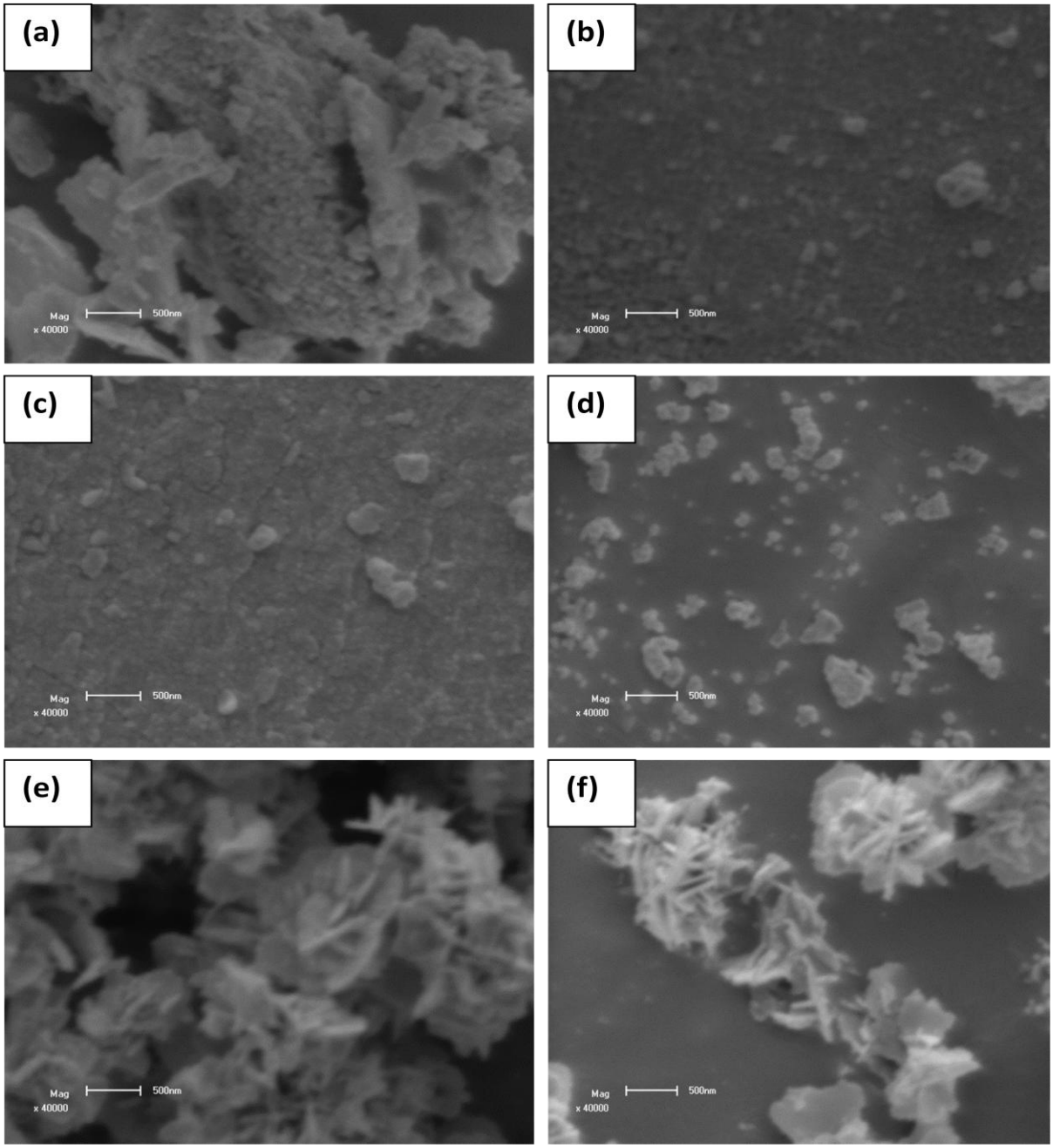

Figure 6.1: SEM images of ZnO nanoparticles prepared using ethanol (a), (b), methanol (c), (d) or water (e), (f) annealed at different temperature 300 °C and 600 °C.

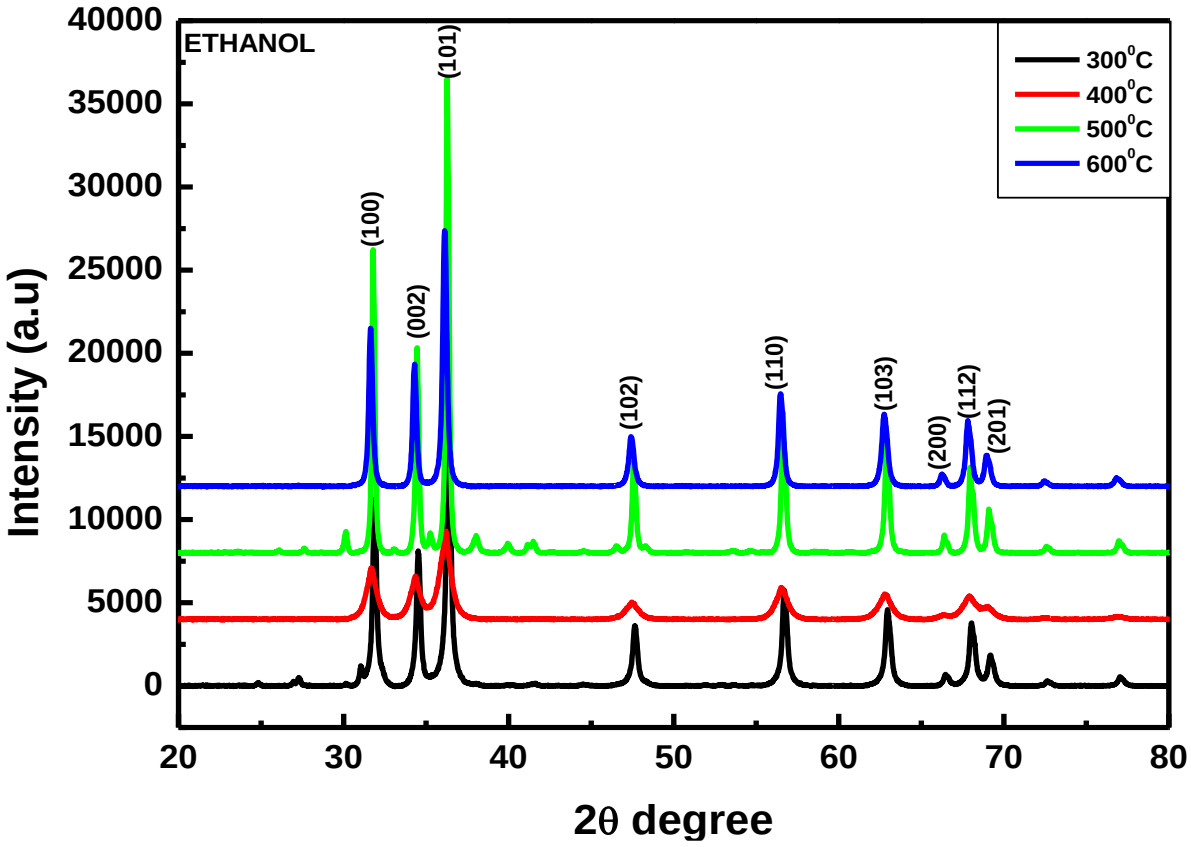

Figure 6.2: XRD pattern of ZnO prepared with ethanol at different annealing temperature (a) 300 °C (b) 400 °C (c) 500 °C and (d) 600 °C.

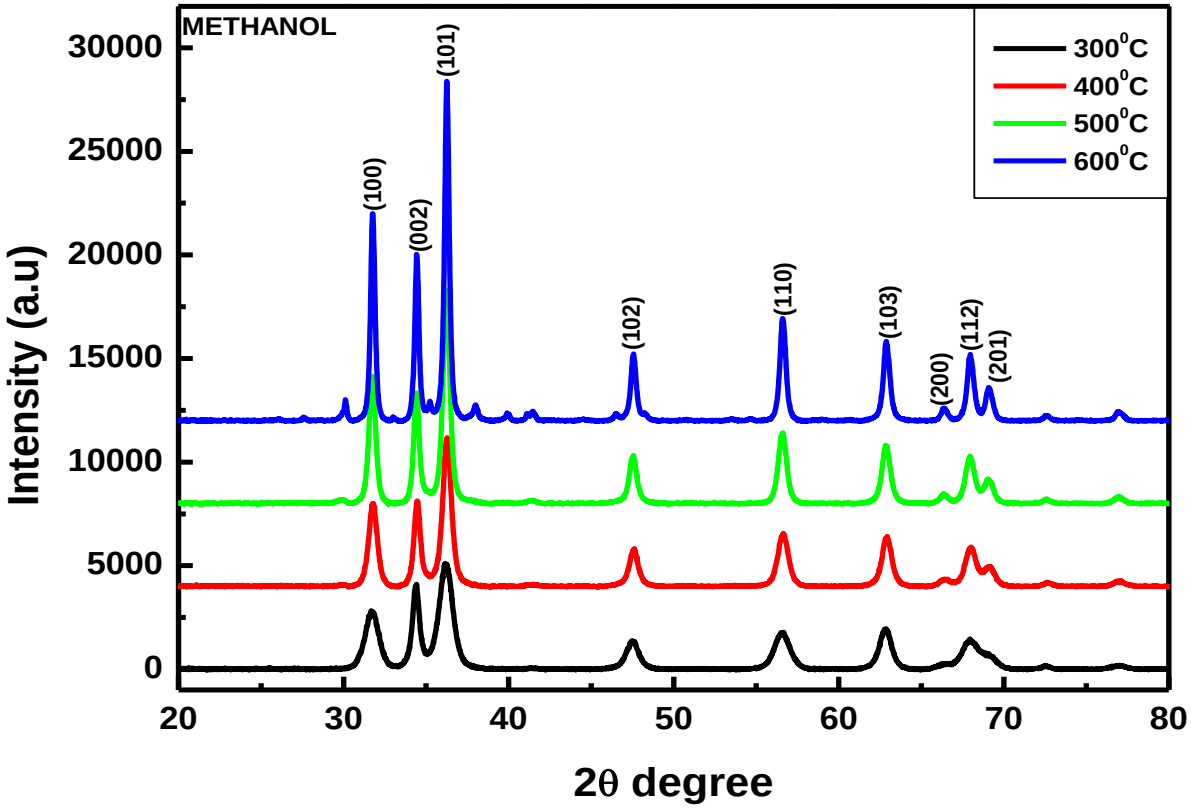

Figure 6.3: XRD pattern of ZnO prepared with methanol at different temperature (a) 300 °C (b) 400 °C (c) 500 °C and (d) 600 °C.

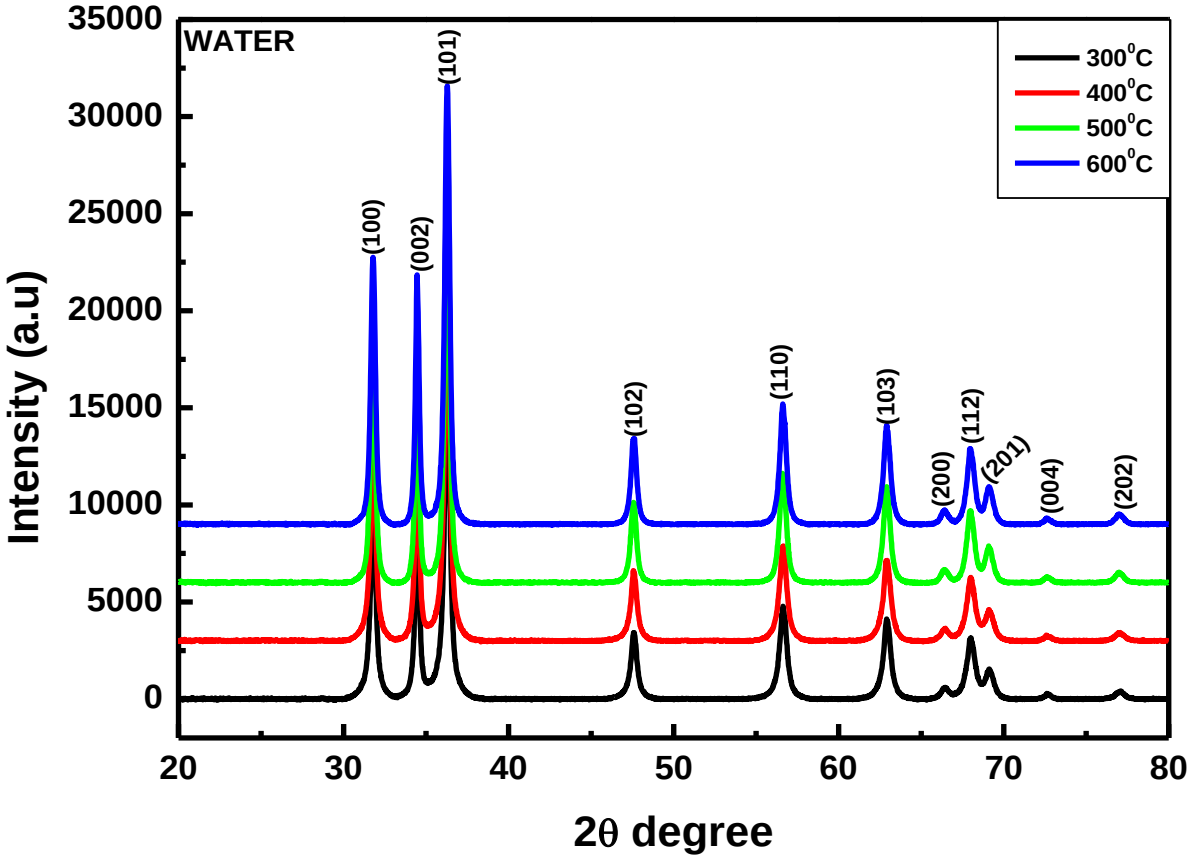

Figure 6.4: XRD spectra of ZnO prepared with water at different temperature (a) 300 °C (b) 400 °C (c) 500 °C and (d) 600 °C.

The crystallite size of all the spectra were calculated using the Debye Scherer formula

$$D = \frac{0.9\lambda}{\beta_{1/2} cos\theta}$$

Where all the symbols have their own meanings that is; D is the diameter of the crystallites, λ is the x-ray wavelength (1.5406 Å), β is the peak width at half maximum (FWHM) and θ is the Bragg diffraction angle. The results revealed that the crystallinity degree fluctuated with the calcination temperature. This was observed with the ZnO prepared using ethanol.

Table 1: The calculated lattice parameters and the grain size of the ZnO nanostructure prepared using (a) ethanol, (b) methanol and (c) water at various annealing temperatures.

(a)

Temperature (°C)	Grain size (nm)	a (Å)	c (Å)
300	58	3.2374	5.1886
400	68	3.2607	5.2116
500	80	3.2452	5.1987
600	62	3.2611	5.2209

(b)

Temperature (°C)	Grain size (nm)	a (Å)	c (Å)
300	24	3.2525	5.2083
400	20	3.2642	5.1769
500	32	3.2520	5.2015
600	48	3.2489	5.2001

(c)

Temperature (°C)	Grain size (nm)	a (Å)	c (Å)
300	38	3.2476	5.1968
400	38	3.2479	5.1971
500	44	3.2483	5.1992
600	46	3.2471	5.1986

All the samples presented crystallite size less than and equal to 80 nm. The particle calculated sizes are in the range 20–80 nm. The values tabulated in Table 1 are close to those of lattice constants a = 3.249 Å and c = 5.20661 Å in the standard data. It was observed from the tabulated table that the grain sizes of the ZnO prepared using water increases with an increase in the annealing temperature the same occurred for the ZnO prepared using methanol.

6.3.2 Optical properties

Presented below are the PL emission spectra for the ZnO nanoparticles prepared using various solvents with excitation wavelength of 230 nm. The spectra of ZnO prepared using ethanol shows a weak UV emission band at ~366 nm, strong blue emissions around 424 - 430 nm. There is a blue shift in the peaks position depending on the calcination temperatures (400 and 500 °C). A strong intensity was observed at an annealing temperature of 600 °C which proves that the temperature has an impact on the preparation of the ZnO. The strong intensity might be due to the various solvents involved in the preparation of the ZnO. This means that the solvents have taken control over the surfaces of the ZnO. It is commonly known that a green-yellow emission is observed in PL spectra due to recombination of photo generated holes with singly ionized charge state of specific defect [9]; however the absence of green-yellow and orange-red emissions in the sample indicates the potential to produce a low concentration of oxygen defects and high optical quality of crystalline ZnO.

The weak green emission of the ZnO prepared using water corresponds to the singly ionized oxygen vacancy in ZnO, and this emission results from the recombination of a photo-generated hole with the singly ionized charge state of the specific defect [10]. Although annealed at various temperatures (300, 500, 600 °C) the spectra of the ZnO prepared using water consist of three emission peaks: a strong emission peak at ~423 nm, a blue-green emission band at ~486 nm, a weak green emission peak at 535 nm. The spectrum of ZnO annealed at 400 °C shows a strong emission peak at ~381 nm. The weak blue-green emissions might be due to surface defects in the ZnO powder as in the case of ZnO nanowires reported by Wang and Gao [11]. An increase on the annealing temperature brings the oxygen and zinc atoms to move from interstitial to lattice sites.

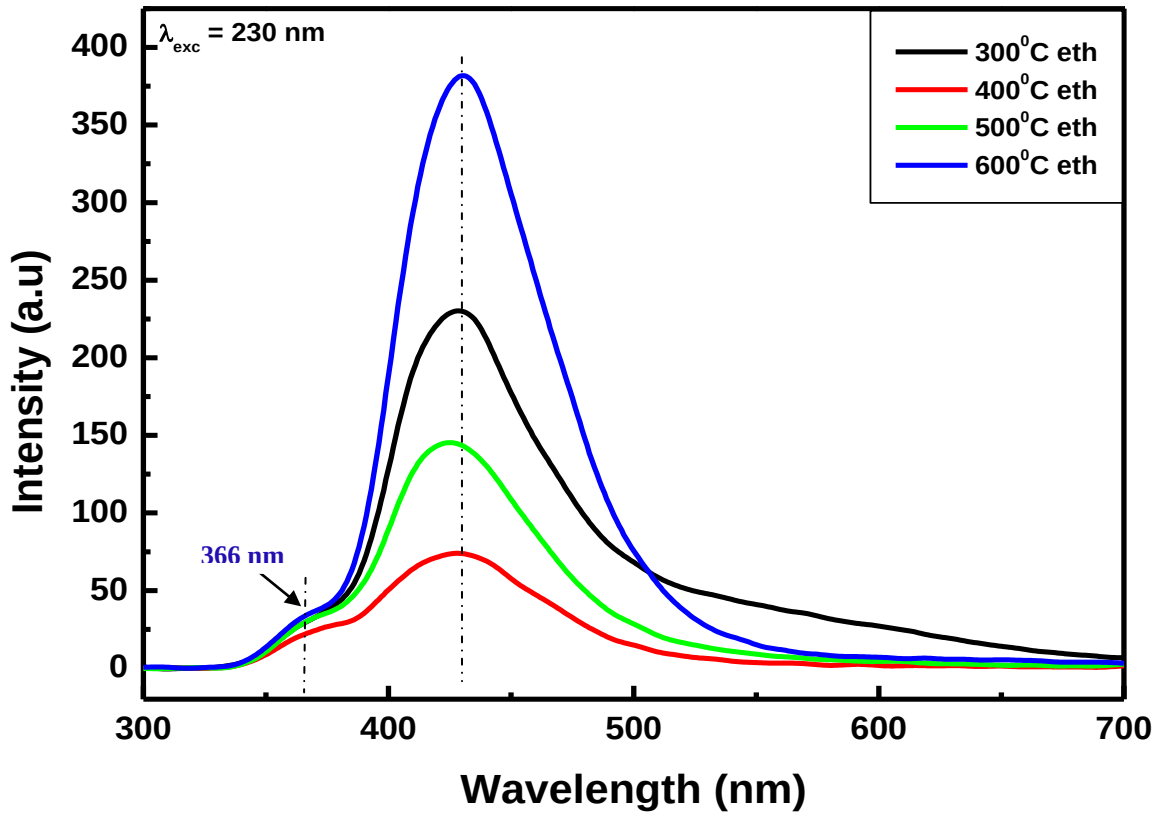

Figure 6.5: PL emission spectra of ZnO prepared with ethanol annealed at various temperatures.

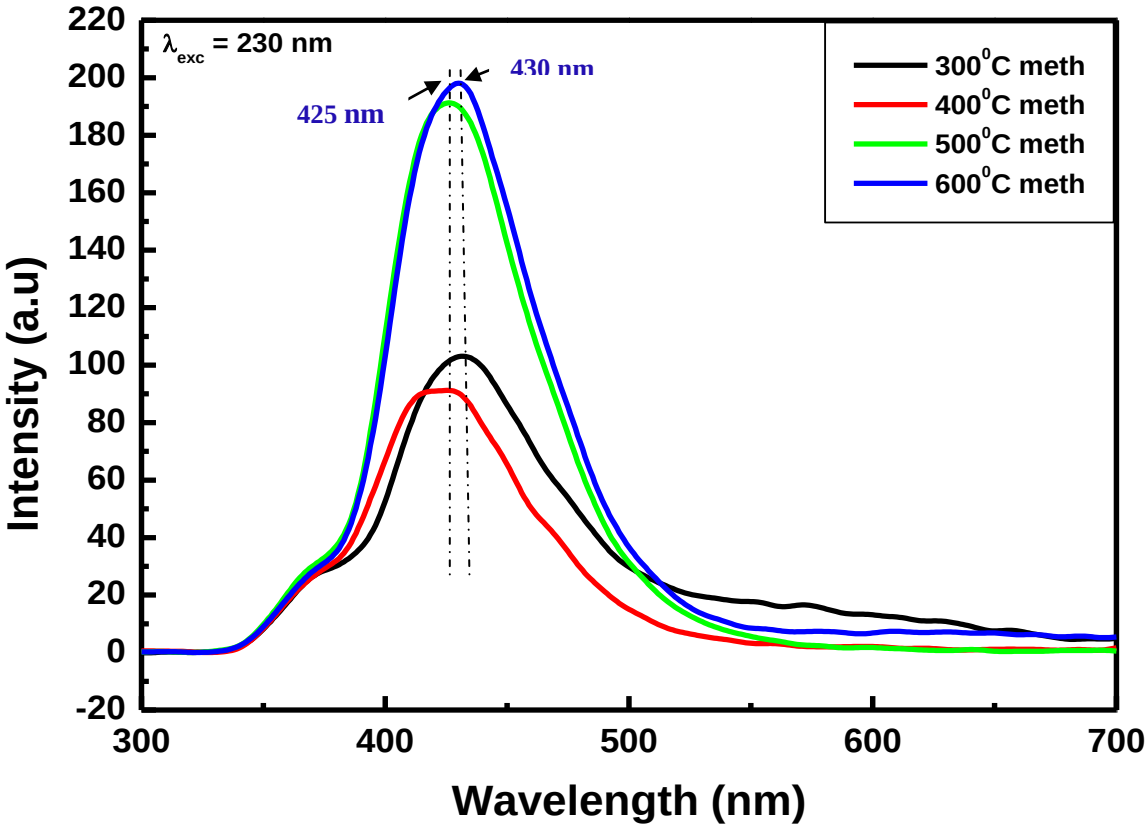

Figure 6.6: PL emission spectra of ZnO prepared with methanol annealed at different temperatures.

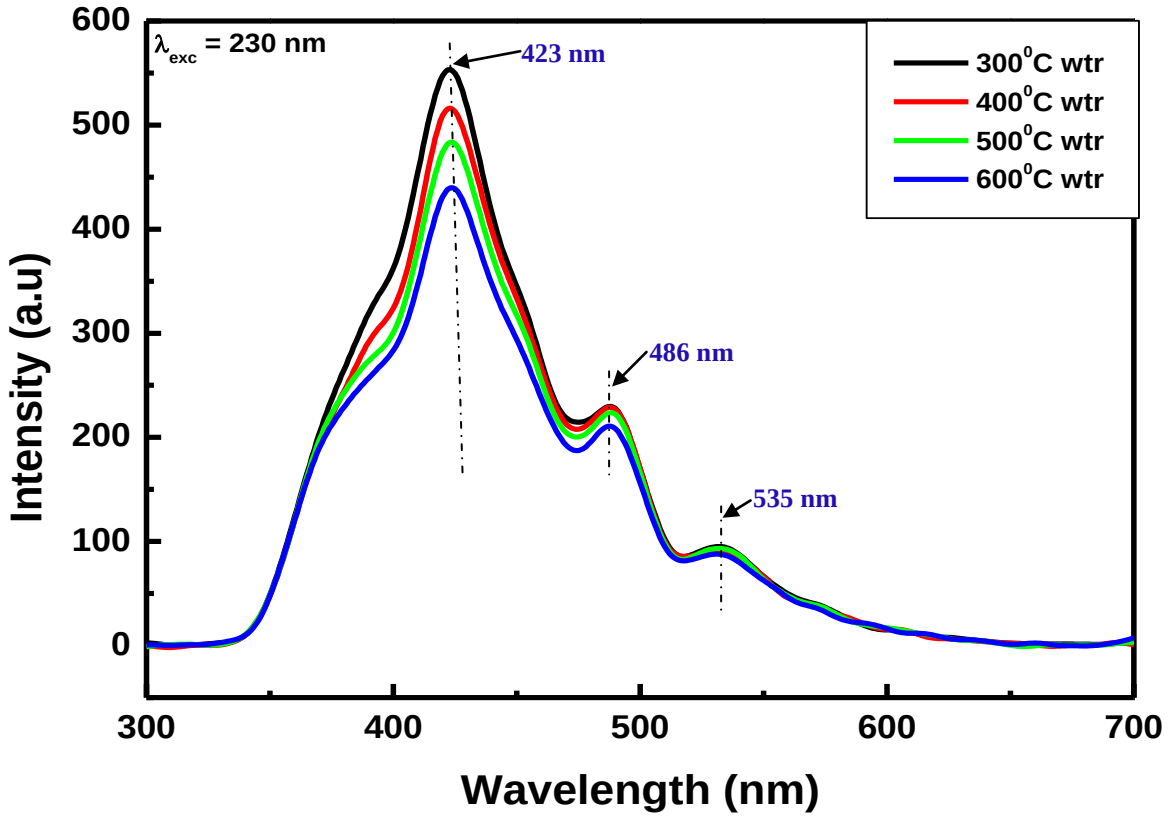

Figure 6.7: PL emission spectra of ZnO prepared with ethanol annealed at different temperatures.

Optical absorption spectra for ZnO prepared using ethanol, methanol or water as solvents are presented in Figures 6.8, 6.9 and 6.10. The UV absorption spectra of the ZnO prepared using ethanol showed the absorption peak centred at 375 nm (~3.30 eV) at an annealing temperature of 300 °C and it is known that the bulk ZnO has an absorption band edge at 375 nm in the UV-visible spectrum [12]. But other spectra of the ZnO prepared using ethanol have no peaks at annealing temperatures around 400, 500, and 600 °C, which is attributed to that the ethanol has taken control over the surfaces of the ZnO. The direct band gap of ZnO nanoparticles was determined by plotting $(\alpha h\nu)^2$ as a function of energy, and extrapolating the linear portion of the curve to absorption gives the direct band gap between 4.2 – 4.7 eV. It was observed that the band gap of the ZnO prepared using ethanol, increases with temperature.

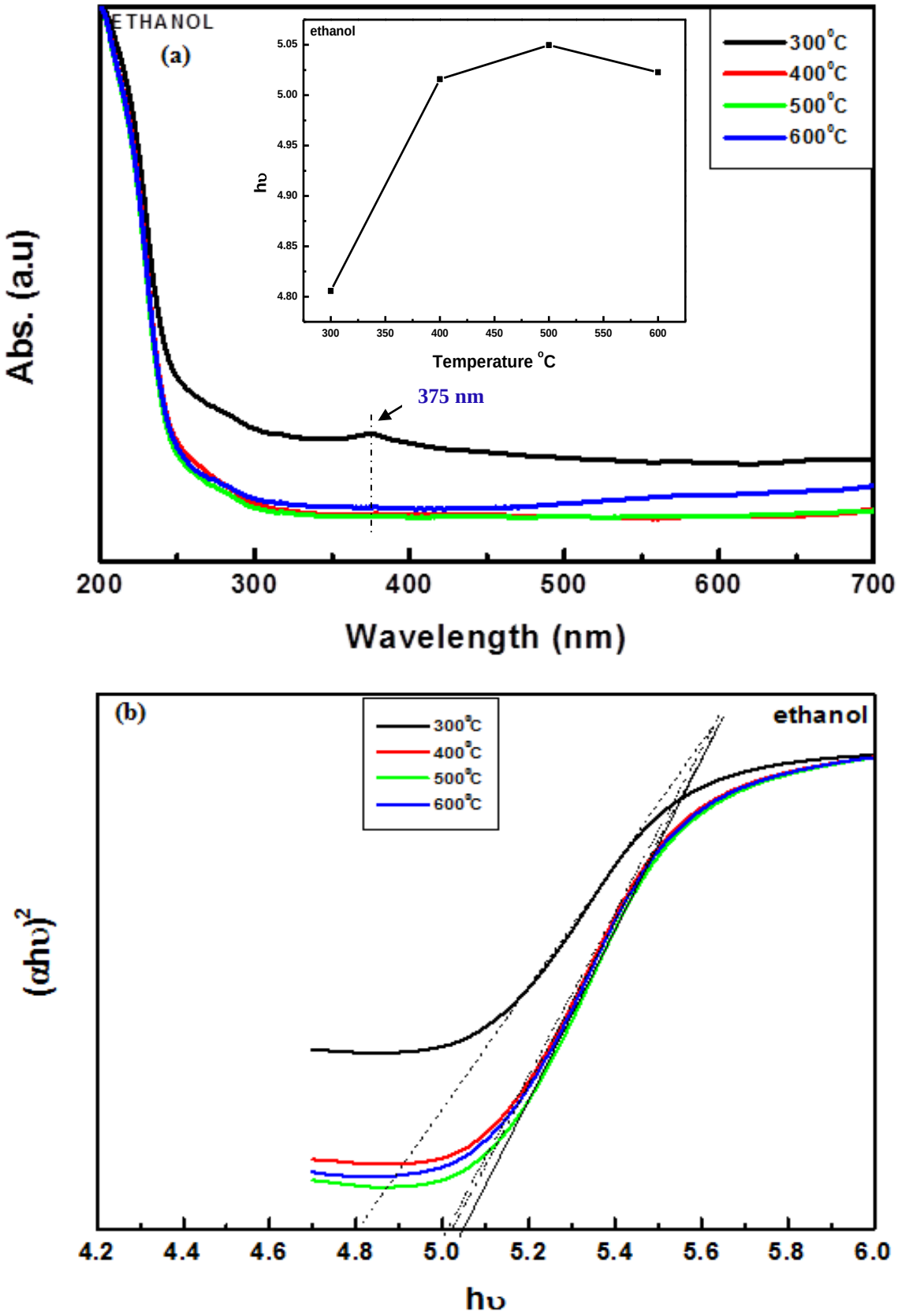

Figure 6.8: (a) Absorption spectra of ZnO nanoparticles prepared with ethanol annealed at different temperatures and (b) plot of $(\alpha h\nu)^2$ as a function of photon energy, E_g annealed at various temperatures.

There are three absorption peaks in the ZnO prepared using methanol that is at ~283 nm, 230 nm. The samples for the annealing temperatures of 300, 500, 600 °C shows and absorption peaks at ~260 nm. ZnO prepared using water exhibits absorption ZnO nanorods, which gives out a blue-shift in the band-edges with an increase in the annealing temperature. The absorption spectra of the products synthesized with water show that the absorption peak gradually shifts from 371, 373, and 375 nm with the increase of the temperature from 300 to 600 °C. The absorption for the ZnO prepared using water decreases with an increase in the annealing temperature. The transmittance of ZnO nanoparticles in the visible region increases with annealing temperature.

The ZnO prepared using methanol shows an increase on the band gap as shown on the insert in Figure 6.9 (a). This increase is due to the increase on the annealing temperature (300, 400, 500 °C). It was observed that at an annealing temperature of 600 °C there was a drop on the band gap. The band gap of the ZnO prepared using water gave the band gap of about 4.59, 4.95 and 5.02 eV at temperatures 300, 400, 500, 600 °C, respectively.

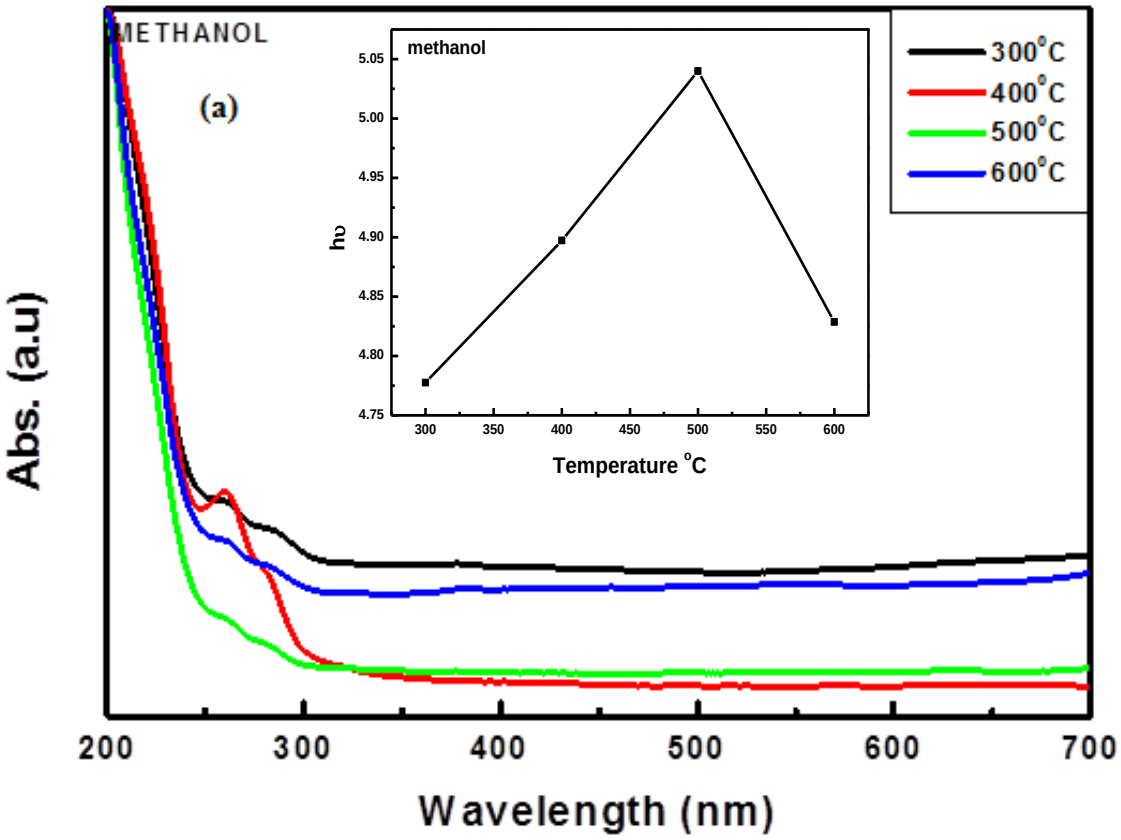

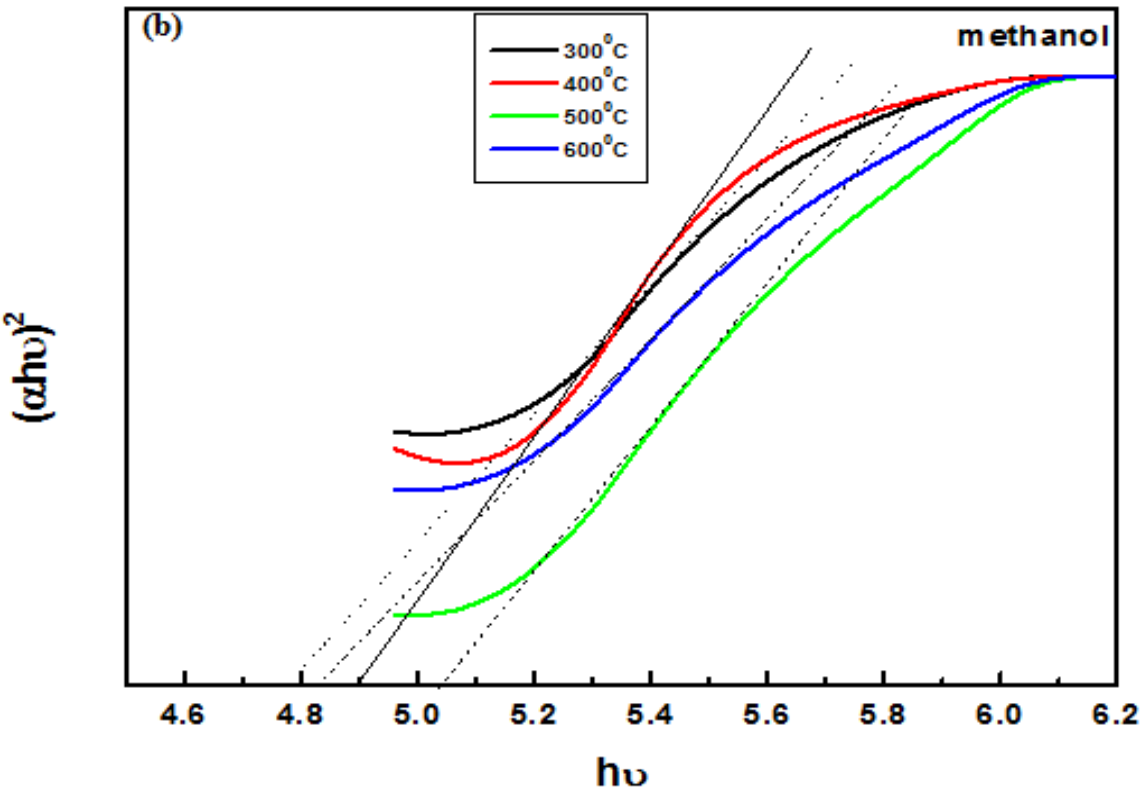

Figure 6.9: (a) Absorption spectra of ZnO nanoparticles prepared with methanol annealed at different temperatures (b) Plots of $(\alpha h\nu)^2$ vs. $h\nu$ for ZnO prepared using methanol with increase in the temperature.

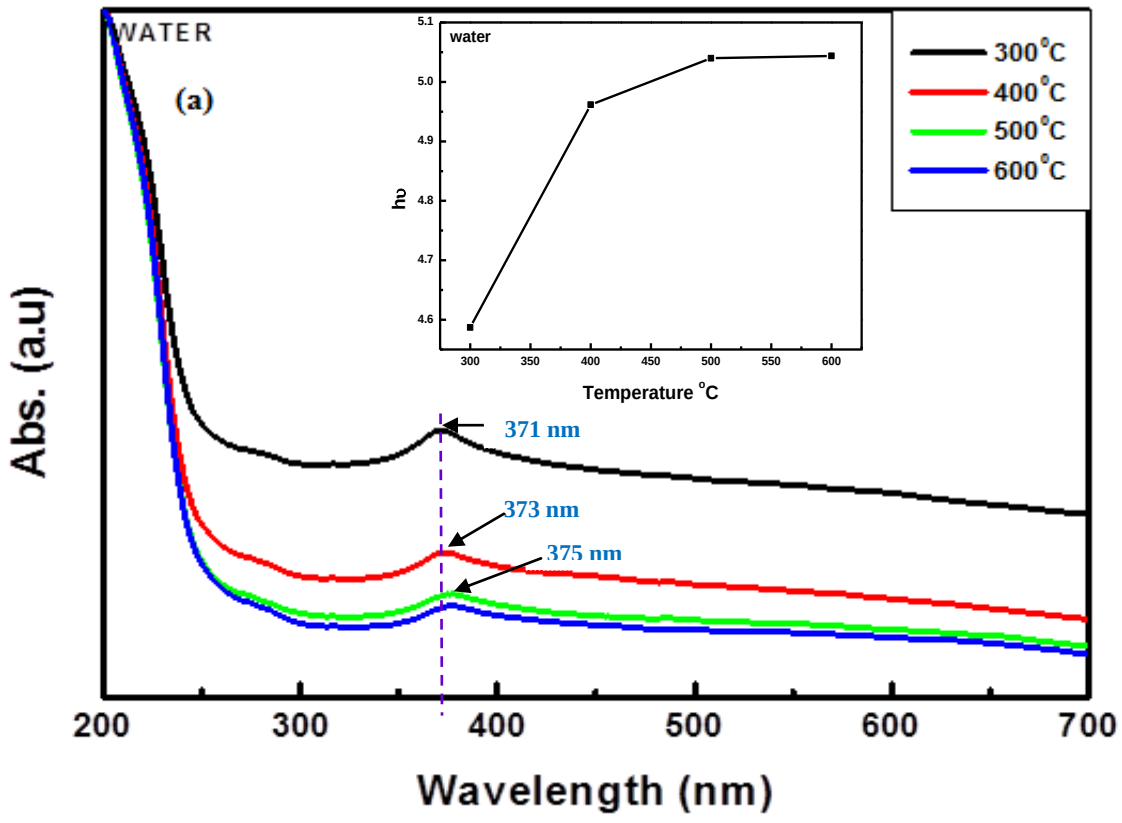

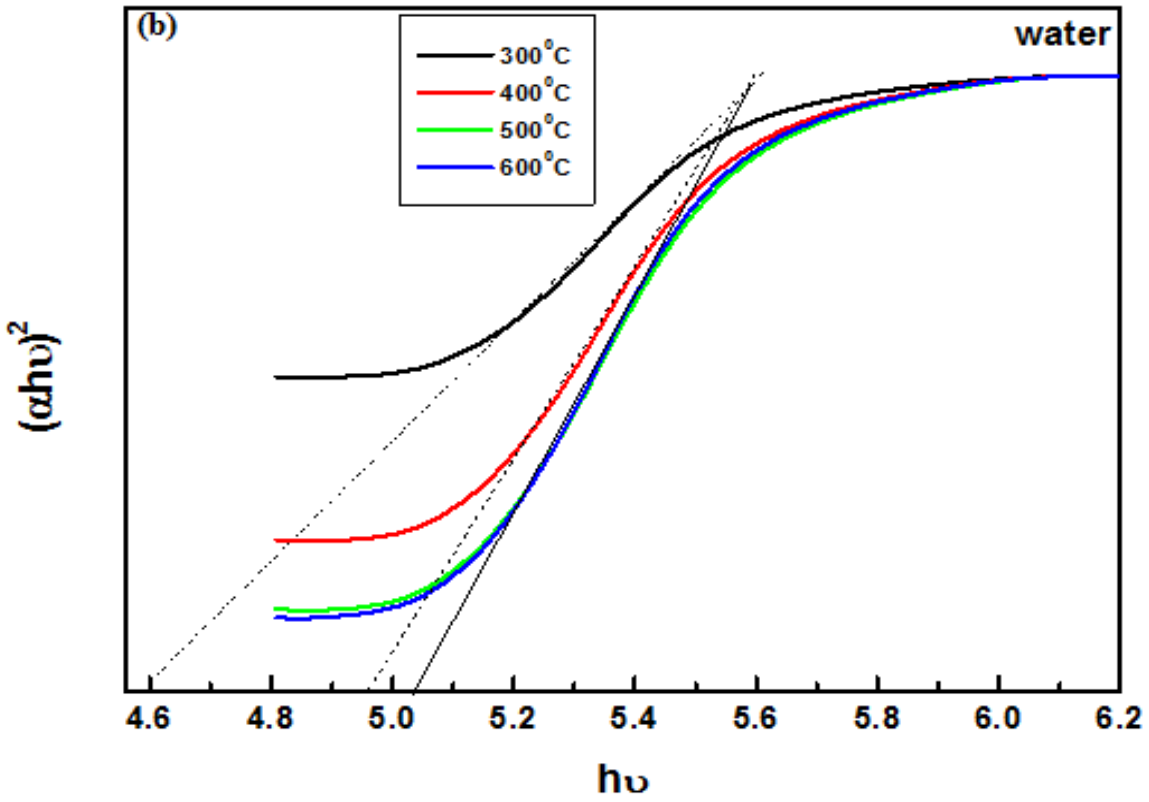

Figure 6.10: (a) Absorption spectra of ZnO nanoparticles prepared with water annealed at different temperatures (b) Plots of $(\alpha h\nu)^2$ versus photon energy at different temperatures.

6.4 Conclusion

In this report, ZnO nanostructures with various shapes and sizes were prepared by sol-gel process. SEM observation revealed nanorods and nanoparticles of ZnO depending on the annealing temperatures of the precursors. XRD showed the impact that temperature has on the structure of the ZnO and for all the solvents the XRD spectra were indexed as that of the hexagonal wurtzite structure. The photoluminescence spectra varied with different temperatures with respect to the solvents used to prepare the ZnO nanoparticles. The UV-vis absorption exhibited various absorption peaks for various solvent when annealed at different temperatures. The plot of $(\alpha h\nu)^2$ versus photon energy of the ZnO was drawn and the band gap was able to be determined. The band gap of the ZnO increased with an increase in the annealing temperatures.

References

[1] L. Sun, Y. Li, N. Miyatake, H. Sue, *J. Sol-Gel Sci Technol* **43** 237-243 (2007)

[2] U. Koch, A. Fojtik, H. Weller, A. Henglein, *Chem. Phys. Lett.* **122** 507-510 (1985)

[3] D.W. Bahnemann, C. Kormann, R. Hoffmann, *J. Phys. Chem.* **91** 3789-3798 (1987)

[4] M. Haase, H. Weller, A. Henglein, *J. Phys. Chem.* **92** 482-487 (1988)

[5] Z. Hu, G. Oskam and P. C. Searson, *J. Colloid and Interface Science* **263** 454-460 (2003)

[6] J. Zhang, L. Sun, J. Yin, H. Su, C. Liao, C. Yan, *Chem. Mater.* **14** 4172-4177 (2002)

[7] Y. J. Kwon, K. H. Kim, C. S. Lim, K. B. Shim, *J. Ceram. Proc. Res.* **3** 146-149 (2002)

[8] C. Hsieh, *J. Chinese Chem. Soc.*, **54** 31-34 (2007)

[9] C. T. Hsieh, J. M. Chen, H. H. Lin, H. C. Shih, *Appl. Phys. Lett.* **83** 3383-3385 (2003)

[10] S. Maensiri, C. Masingboon, V. Promarak and S. Seraphin, *Opt. Mat.,* **29** 1700-1705 (2007)

[11] J. Wang, L. Gao, *Solid State Commun.,* **132** 269-271 (2004)

[12] D. Yiamsawas, K. Boonpavanitchakul, W. Kangwansupamonkon, *J. Microscopy Society of Thailand*, **23** 75-78 (2009)

CHAPTER 7

Influence of pH value on the material properties of the ZnO nanostructures using various solvents at constant temperature

7.1 Introduction

Zinc oxide ZnO is a wide direct band-gap 3.37 eV semiconductor with a broad range of applications including light-emitting devices [1], varistors [2], solar cells [3], and gas sensors [4]. Preparation of nanosized ZnO has been carried out by different methods such as micro-In this work the sol-gel process were used to prepare the ZnO nanoparticles using various solvents. This method was chosen because of its advantages that are its inexpensive, reliable, repeatable and simple. It is known that the nanoparticles are highly sensitive to surface environments such as water, moisture, humidity, pH and solvents [5]. The pH affects the hydrolysis and condensation behaviour of the solution during gel formation and therefore influences the morphology of the ZnO. In this paper, we report the role of pH value on the structural and optical properties of ZnO nanoparticles. NaOH was used to vary the pH values from 10 to 13.54. The morphology and structure of the grown samples can be controlled by adjusting parameters such as the temperature, the concentration of the solution, the stoichiometry of the reagents and pH [6]. The optical properties usually depend on the shape and size of ZnO crystal. The pH of the solution is one of the important factors that influence the ZnO properties when synthesizing ZnO by the sol-gel route. The pH has an impact on the condensation and hydrolysis behaviour of the solution during the formation of the gel and then influences the morphology of the ZnO [7]. In this section, we investigate the morphology, crystal structure, and band gap and emission characteristics of ZnO nanostructures synthesized by the aqueous chemical growth technique using different solvents. The effect of the pH on the properties of the ZnO was also investigated.

7.2 Experimental procedure

4.3898 g of $Zn(Ac)_2$ was first dissolved in 100 mL ethanol with continuous stirring until homogeneous solution was obtained. 3.2 g of NaOH was dissolved in different volumes of ethanol, methanol or water and added slowly into the zinc acetate solution. When mixing the NaOH solution prepared with methanol into the zinc acetate solution, the white precipitates forms and immediately fades away. Continuous addition of NaOH solution leads to a permanent milky solution with precipitates. The mixture was then vigorously stirred at an ambient temperature for an hour before filtering, rinsing with distilled water, drying at 60°C and then calcining at 600°C in air for 1 hour.

After stirring the mixture prepared with methanol for 1 hour, the precipitate faded away. The samples were then left for about 2 days to form two layers, then discarded the top layer and then washed it with distilled water. Then they were then left in a fume cupboard for another 2days to dry up and then calcined at 600°C.

7.3 Results and discussion

7.3.1 Structure and morphology

The morphology and size of the dried ZnO nanoparticles were examined by SEM observations. Figure 7.1 represents SEM images of ZnO prepared with various solvents annealed at a constant temperature. An agglomeration of particles was observed in most of the cases which may be due to the prolong reaction time [8]. SEM images for the ZnO prepared using ethanol and methanol shows the agglomerated spherical ZnO nanoparticles of different sizes that are closely packed together. The agglomeration of these particles may be due to overlapping of smaller particles and might also be due to the alkaline pHs of solutions during the synthesis process.

At a pH value of 10.06, the shape of ZnO nanostructures is different as compared to the pH value of 13.54, which indicates that pH value is important parameter to the morphology of ZnO. ZnO prepared using methanol at pH 13.54 shows the granular structure with nanoparticles on top of them.

The SEM images for the ZnO prepared using water also presented the agglomerated particles at a pH 10.06 and at a pH 13.54 showed the ZnO particles clustered together. At a pH of 13.54, the Na^+ has taken control over the surface of the ZnO.

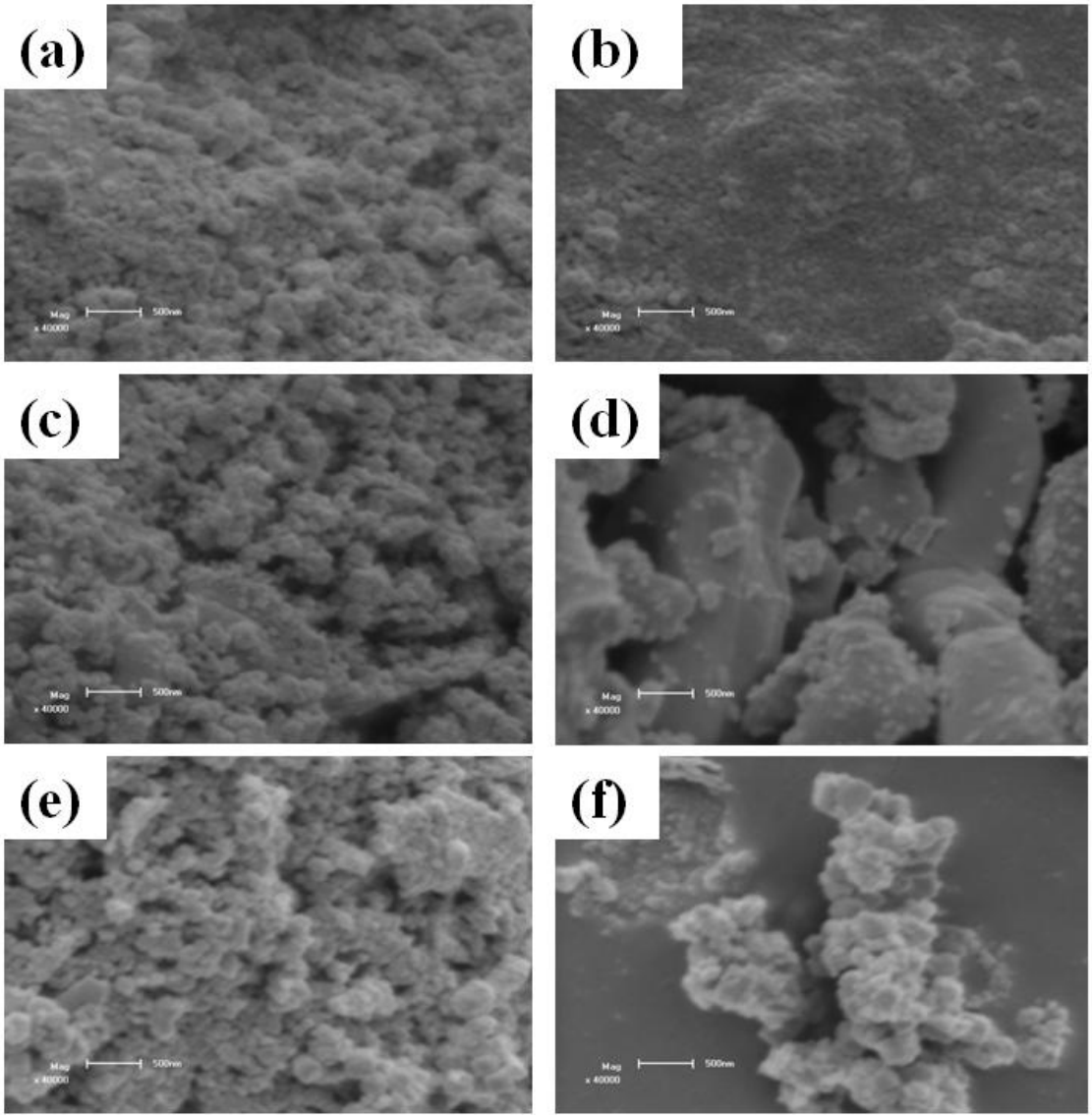

Figure 7.1: SEM images of the ZnO prepared using (a) and (b) ethanol, (c) and (d) methanol and (e) and (f) water at pH values of 10.06 and 13.54.

Table 1: The calculated and measured lattice parameters for the ZnO prepared with ethanol.

		Lattice parameters	
pH	Grain size (nm)	a (Å)	c (Å)
10.06	72	3.235	5.2024
11.08	68	3.237	5.1964
12.81	56	3.364	5.1821
13.34	38	3.252	5.1982
13.54	34	3.323	5.1894

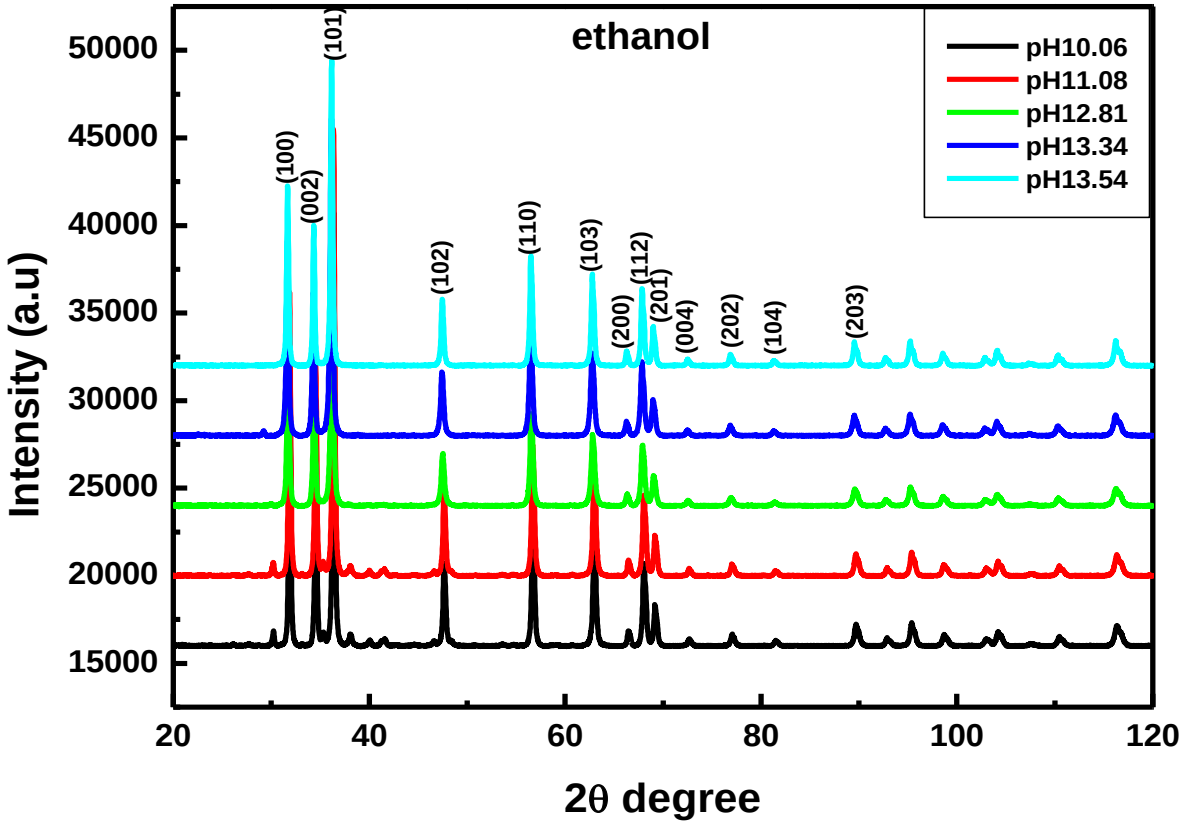

Figure 7.2: XRD spectra for the ethanol prepared ZnO at various pH values.

The XRD patterns of all samples of ZnO powder obtained at different pH value are shown in Figure 7.2 – 7.4. The powders showed three major peaks corresponding to (100), (002), and (101) planes which are indexed as JCPDS card no. 36-1451 for ZnO hexagonal wurtzite structure materials, which indicate that the samples are polycrystalline. Other peaks were shown that also corresponded to the standard card number. The sharpness of the peaks shows

the crystallinity of the samples. XRD spectra for ZnO prepared with both ethanol and methanol show small peaks that are not on the JCPDS.

It has been revealed from the ZnO prepared using water that the peak intensity at pH 13.54 is shown to be the lowest this is due to an increase on the addition of NaOH. As the pH increases, the intensity of the reflections peaks decreases as seen from Figure 7.4. The highest intensity peak appears at pH 10.06 because enough amount of OH^- is available to ZnO. It is observed that the full width at maximum of the diffraction peaks of the ZnO products varies in the large range indicating the crystal sizes of the ZnO products are rather different from each other. From Table 3, the lattice parameters calculated for the ZnO synthesized with water, which did not show much of a difference as compared to the ZnO hexagonal wurtzite structure.

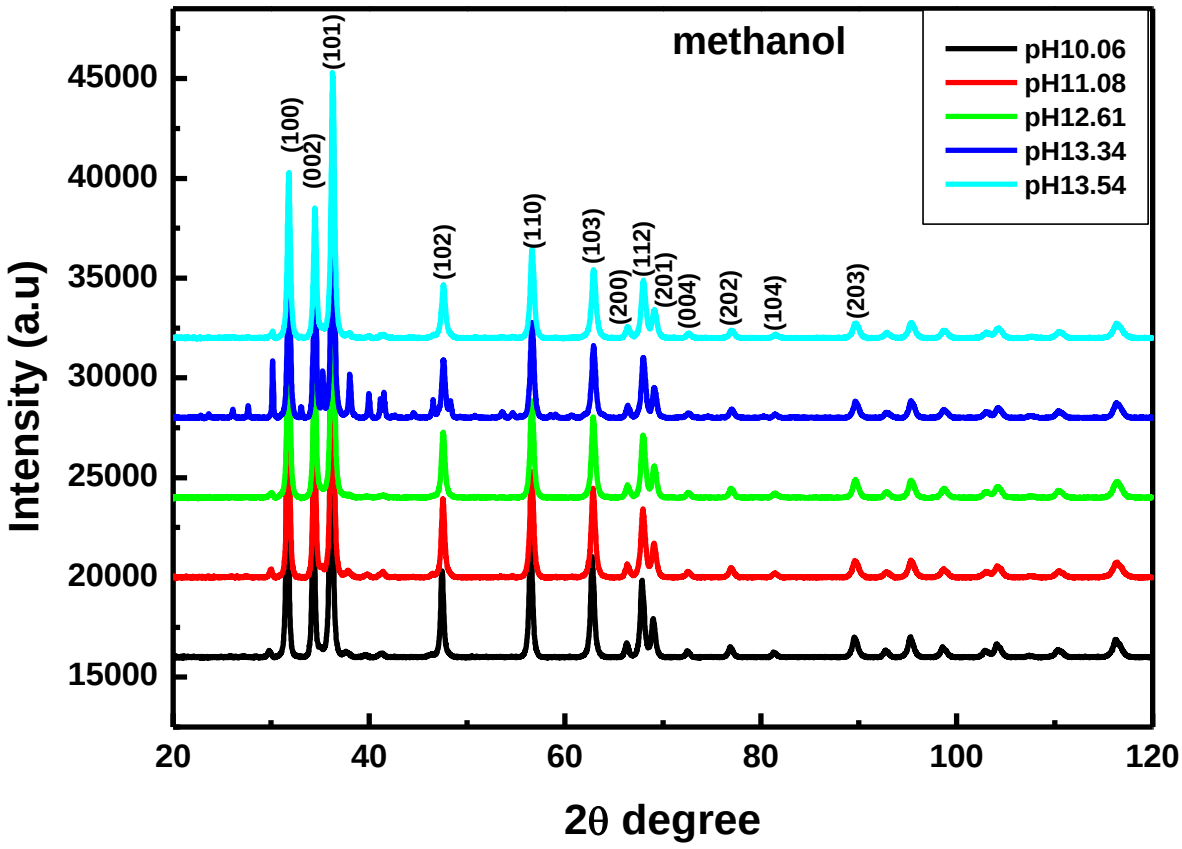

Figure 7.3: XRD spectra for the methanol prepared ZnO at various pH levels.

Table 2: The lattice parameters for the ZnO prepared with methanol at various pH values.

		Lattice parameters	
pH	**Grain size (nm)**	**a (Å)**	**c (Å)**
10.06	54	3.258	5.219
11.08	64	3.290	5.192
12.61	76	3.249	5.158
13.34	90	3.255	5.514
13.54	60	3.323	5.230

The ZnO prepared using methanol has also given the hexagonal wurtzite structure but with extra peaks at angle around 30.15 °C and at a range 36 - 47°C. These small peaks are due to the impurities. There is a decrease on the (102) peak intensity with an increase on the pH that is the addition of the NaOH solution. From the Figures, the difference on the full width at half maximum of the diffraction peaks were observed, indicating that the crystal sizes of the ZnO powders synthesized in methanol are rather different from each other. The reason for this might be various level of the pH in each sample. This can also be seen from the lattice parameters calculated for the ZnO synthesized with methanol (Table 2). The value of lattice parameters a and c were almost close to that of ZnO hexagonal wurtzite structure for the pH 10.06 and 11.08, while the same cannot be said for the pH 12.61 and 13.34.

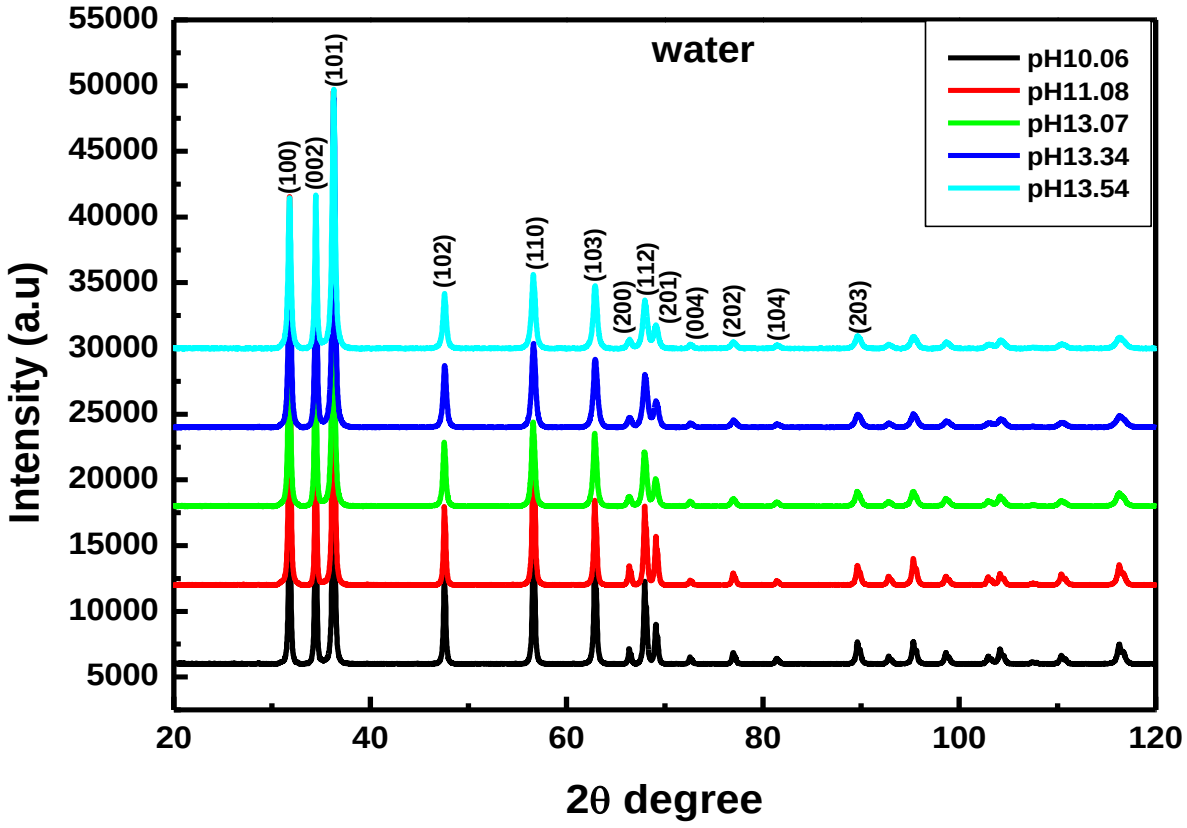

Figure 7.4: XRD spectra for the water prepared ZnO at various pH levels.

Table 3: The lattice parameters for the ZnO prepared using water with various pH values.

		Lattice parameters	
pH	**Grain size (nm)**	**a (Å)**	**c (Å)**
10.06	54	3.229	4.9446
11.08	72	3.246	5.2016
13.07	54	3.249	5.2019
13.34	48	3.246	5.1979
13.54	44	3.129	5.2492

Determination of crystallite size was determined by using the Scherer equation, $D = \frac{0.9\,\lambda}{\beta_{1/2}cos\theta}$, where D is the diameter of the crystallites, λ is the wavelength of Cu K_α line (1.54 Å), and β is full width at half maximum (FWHM), θ is the Bragg diffraction angle. Lattice parameters

were obtained for all the samples as shown on the tables 1, 2 and 3. From table 1, the grain size decreases with an increase on the pH value.

7.3.2 Optical properties

Figure 7.5 shows the PL spectra of all the full ZnO nanostructure samples prepared using ethanol as a solvent. All samples of PL measurements were done at room temperature. It was observed that all ZnO samples show a strong broad blue emission at 428 nm and a weak shoulder in the UV region. The pH of the precursor solution was varied from 12.81 to 13.07 by addition of the NaOH solution. The increase in pH with addition of NaOH clearly indicates an increase of alkaline nature of the prepared solutions. These blue emissions were found to be extremely broad and thus broadness may be due to phonon assisted transition [9]. The emission varied intensity with variation of the pH of each sample while peak position never changed. Figure 7.5 represent the ZnO prepared using ethanol, from this figure the different emissions of various pH values can be seen which was brought by the addition of the NaOH solution. The intensity also decreased with an increase on the pH that is an increase in the addition of the NaOH solution. The lowest intensity was observed for the pH 13.54 while the highest intensity occurred for pH 11.08 when ethanol was used as a solvent.

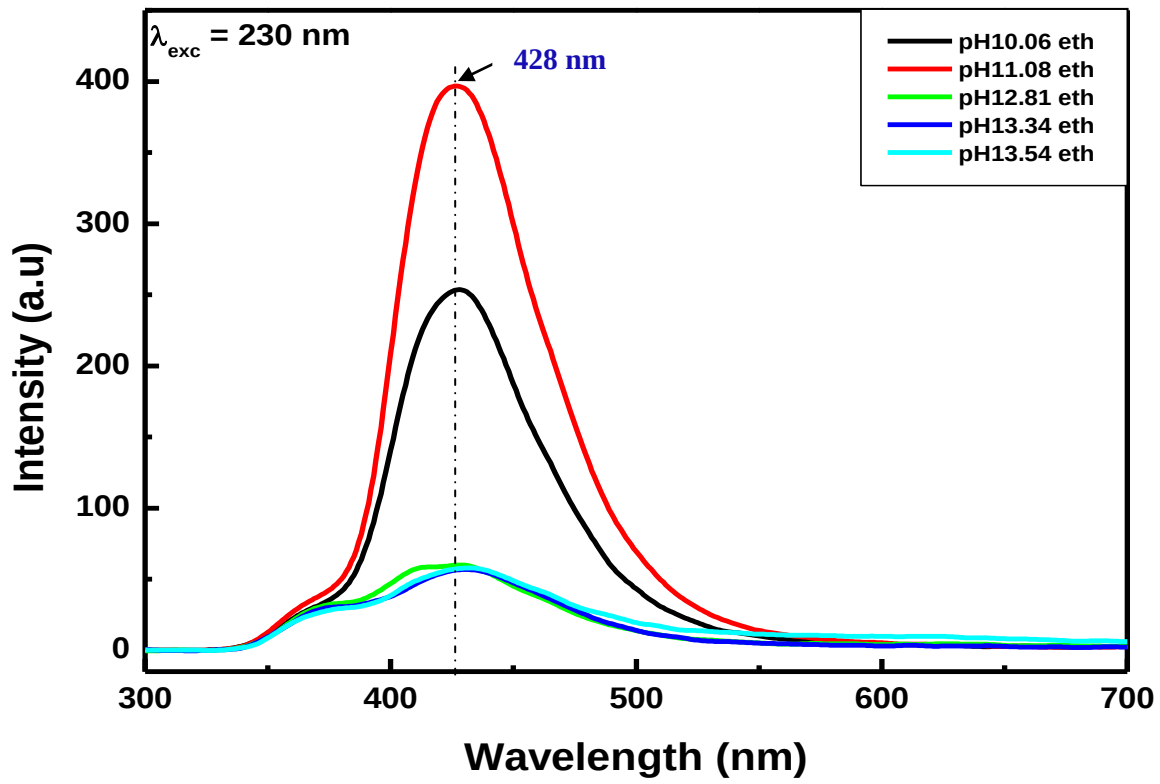

Figure 7.5: PL spectra for the ZnO powders prepared with ethanol at various pH values.

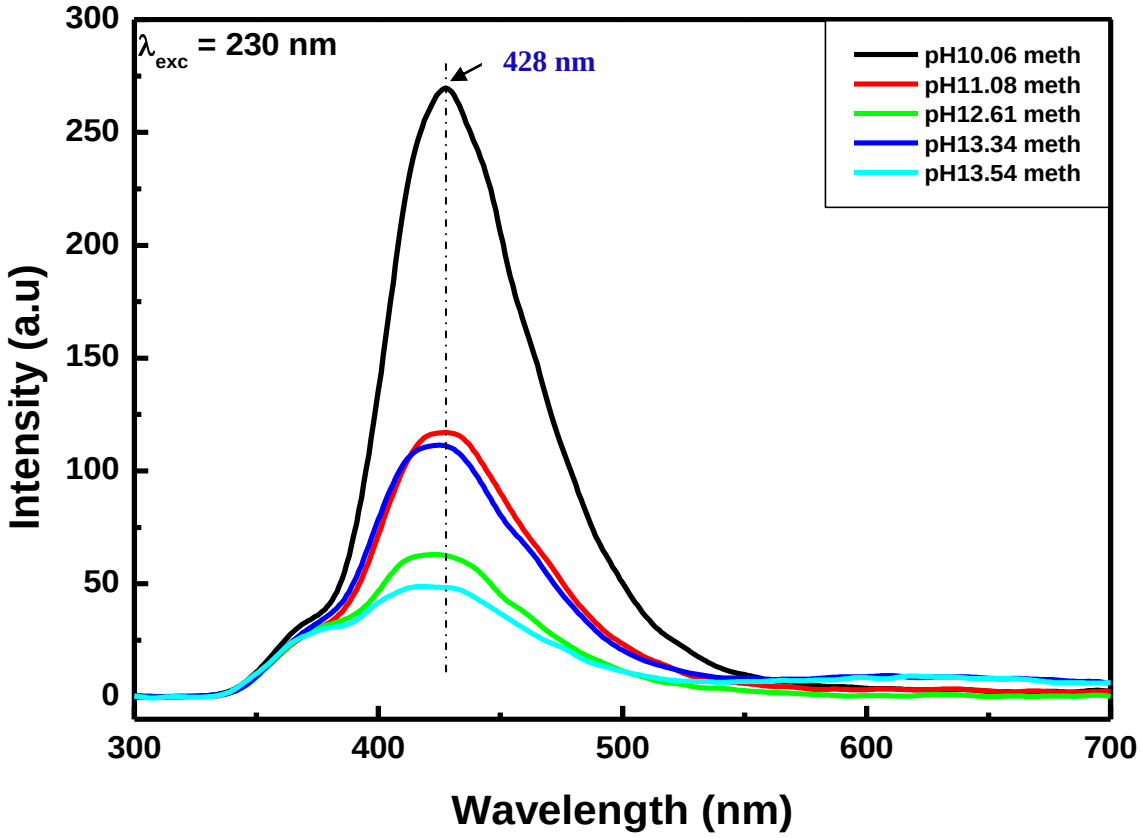

Figure 7.6: PL spectra for the ZnO powders prepared with methanol at various pH levels.

The pH spectra of ZnO prepared using methanol as a solvent is shown in Figure 7.6. A blue emission peak exists for the ZnO prepared using methanol at around 427 nm and a very broad green-yellow peak around 632 nm. The precursor with pH of 10.06 exhibited the stronger luminescence intensity which might be due to the amount of NaOH solution added into the $Zn(Ac)_2$ solution. The pH was observed to significantly affect the peak intensity of blue emission without any effect on peak position.

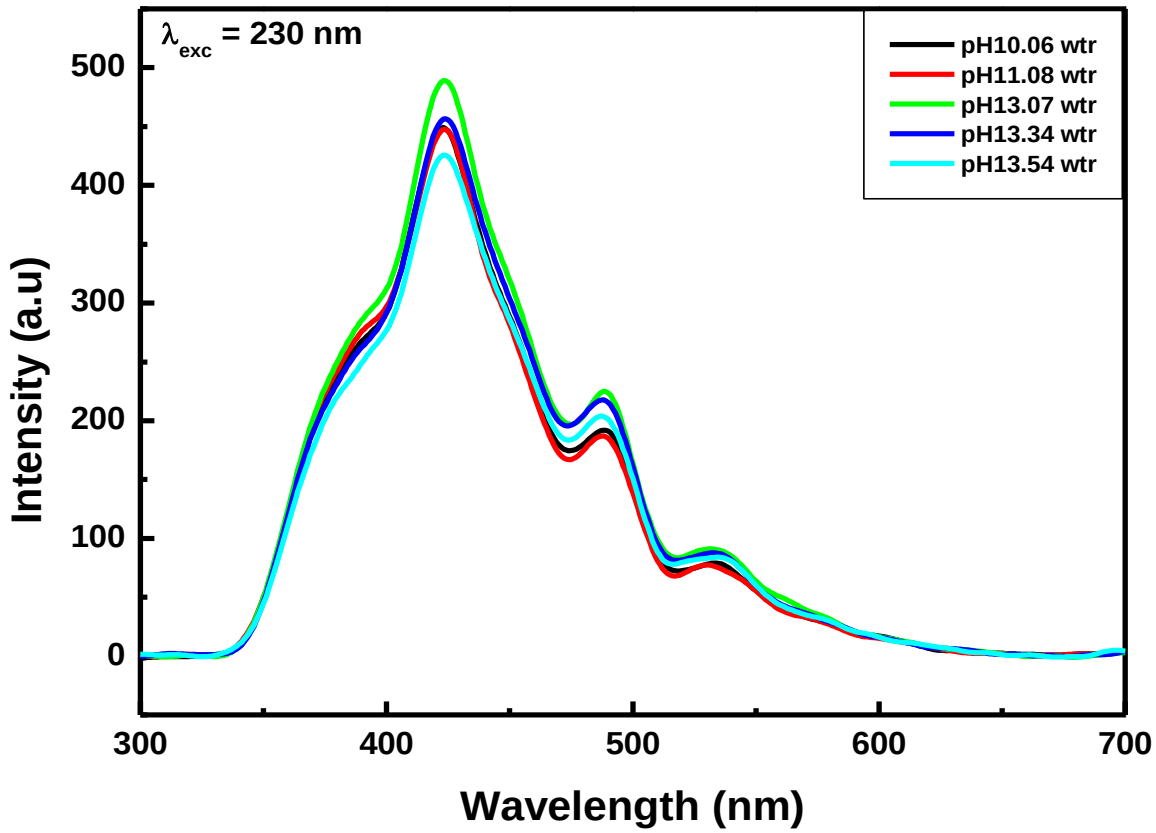

Figure 7.7: PL spectra for the ZnO powders prepared with water at various pH levels.

The ZnO sample prepared using water as a solvent showed three emission bands, a weak ultraviolet emission band at 388 nm, strong blue emission peak at 423 nm, a weak blue-green emission band at 488 nm and a weak green emission band at 533 nm. Green emission in ZnO [10, 11] is commonly observed although other colours have yellow, blue [12] are also reported. The UV emission from the ZnO is generally behaved to be due to exciton emission while emission in the visible range is due to extrinsic or intrinsic defects. The green band emission originates from the transition between the singly ionized oxygen vacancies in ZnO of photogenerated hole [13]. In comparison with other solvents the preparation of ZnO using water as solvent appears to have dependent on the variation pH of the solution.

Below are the UV absorption spectra of the ZnO prepared using ethanol, methanol or water controlling the pH values. The optical absorption coefficients α of the direct band gap semiconductor ZnO can be derived using the following equation

$$(\alpha h\nu)^2 = (h\nu - E_g)$$

Where, hν is photon energy, and E_g is the band gap [14].

All the ZnO samples prepared using various solvents exhibits E_{opt} values larger than that of bulk band gap. This blue shift of the band gap of approximately 1.5 eV (in some cases) can be attributed to quantum confinement caused by nanosized particles clearly. Therefore the present results indicate that the band gap of ZnO nanostructures can be engineered by varying of pH of the precursor solution.

It was observed from the ZnO prepared using ethanol the two absorption peaks. The first absorption band is at ~219 nm and the second one at ~282 nm. At a pH value of 10.06, there is a peak at ~379 nm and this absorption band seems to be suppressed with an increase on the pH values. The suppression clearly means that the Na^+ has taken the whole surface of the ZnO. The absorption of ZnO prepared using ethanol decreases with an increase on the pH values. This is observed for the pH values between 10 and 13.34. The band gap of the ZnO prepared using ethanol increased with an increase on the pH values between 10 and 12.81. When the pH value of solution is equal to 13.34 and 13.54, the band gap starts to decrease. The plotting of photon energy as a function of pH value is inserted in Figure 7.8 (a).

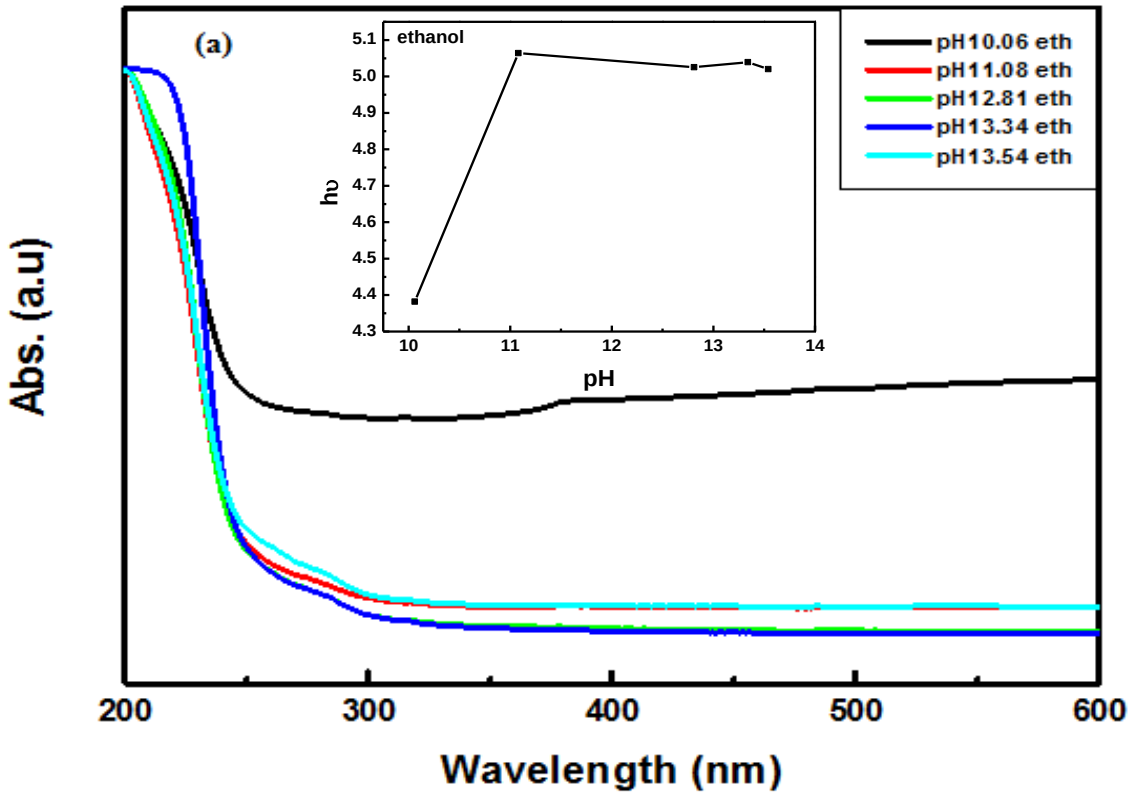

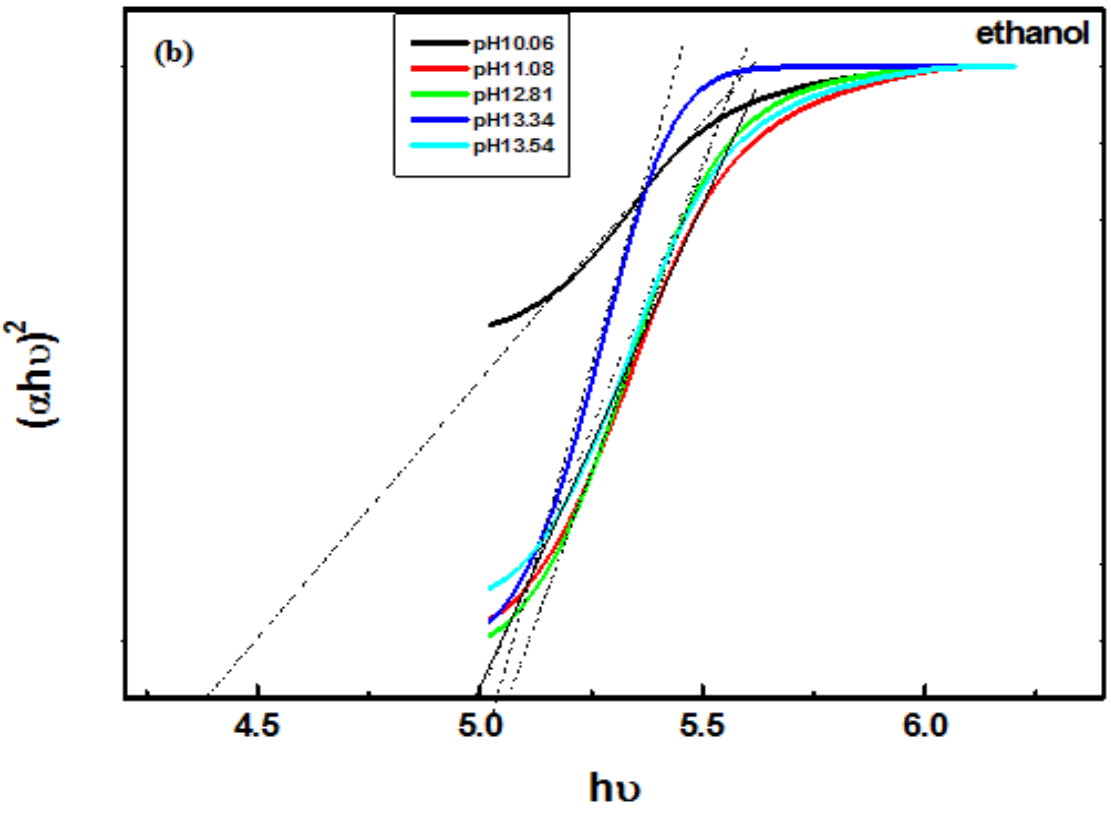

Figure 7.8: (a) UV spectra for the ZnO powders prepared using ethanol at various pH levels (b) Plotting of $(\alpha h\nu)^2$ vs. photon energy.

The UV absorption spectra of the ZnO prepared using methanol show a band edge around 248 nm and a weak peak at around 282 nm for the pH values from 10.06 to 13.34. The pH value 13.54 exhibits two absorption bands at ~260 and 280 nm. It is observed from the band gap spectra that when the pH value is 13.54, the band gap decreases but the same cannot be said for the pH values between 10.06 and 13.34. At this pH range, an increase on the band gap is observed.

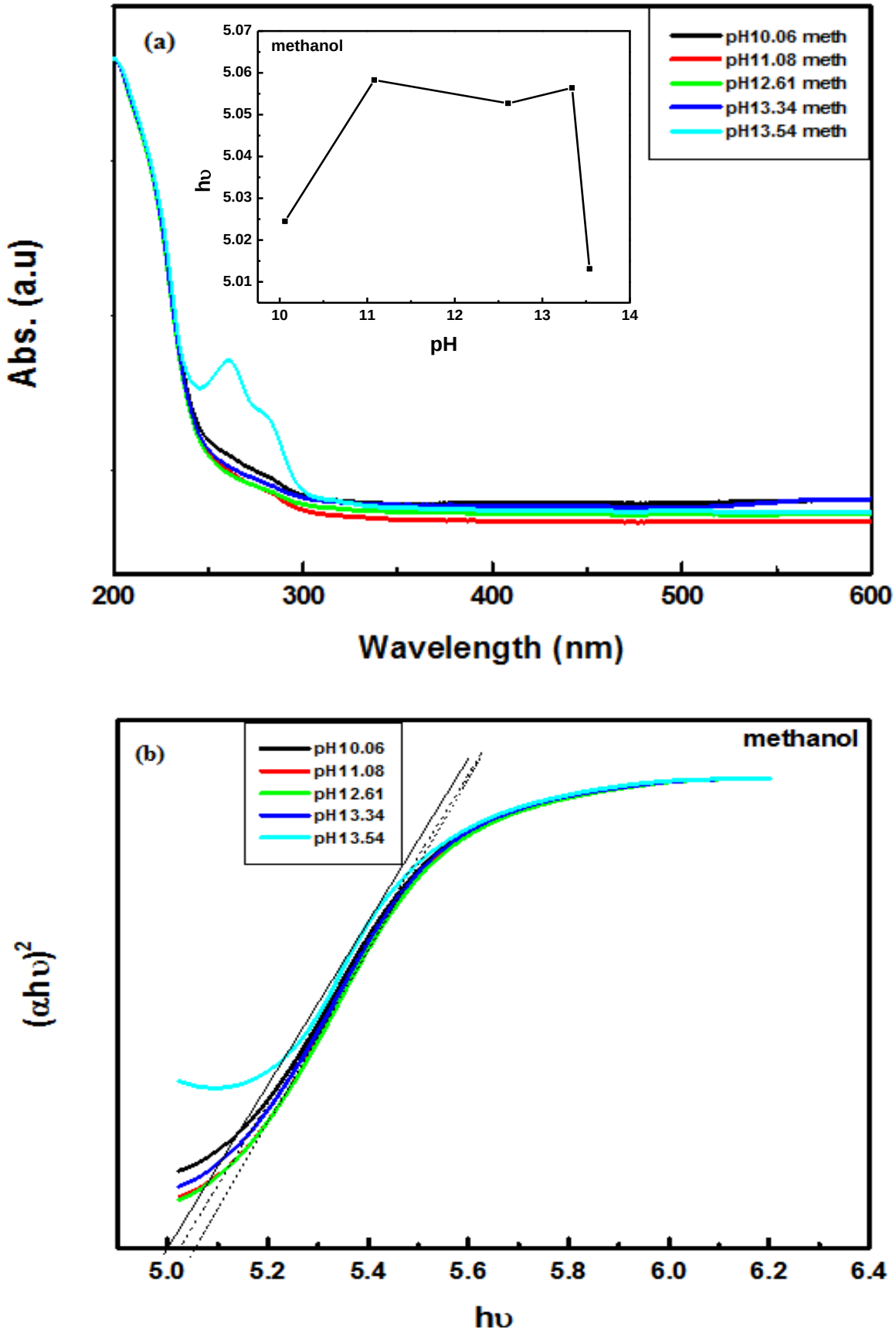

Figure 7.9: (a) UV spectra for the ZnO powders prepared using methanol at various pH levels (b). plot of $(\alpha h\nu)^2$ against the photon energy.

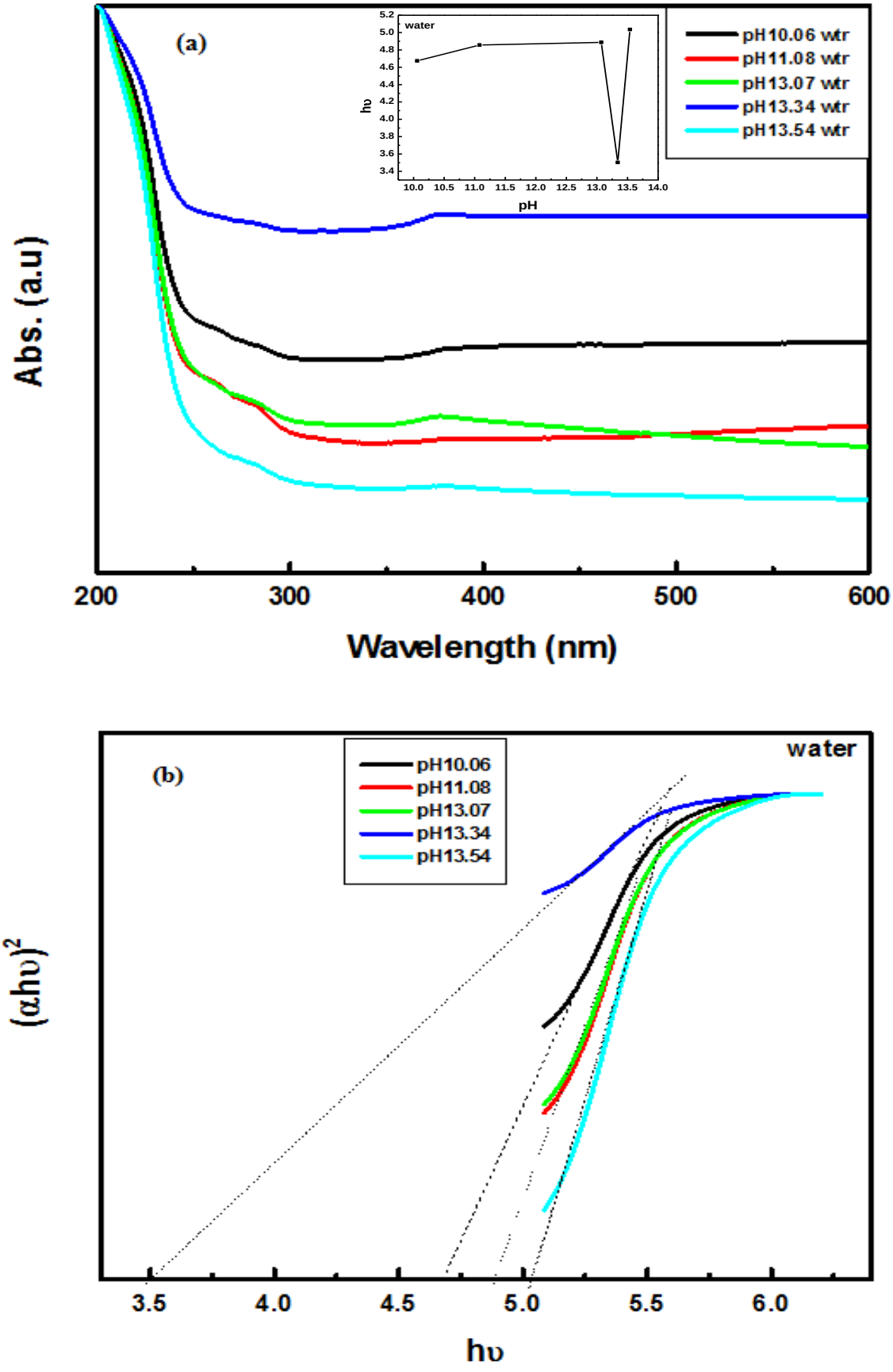

Figure 7.10: (a) UV spectra for the ZnO powders prepared using water at various pH levels (b) plot of $(\alpha h\nu)^2$ against the photon energy.

The ZnO prepared using water showed the UV absorption with band position at a range 376 – 381 nm. The absorption fluctuates with an increase on the pH values. This also applies on the absorption at around 281 nm for all the samples. An increase on the direct band gap on the ZnO prepared using water was observed with and increase on the pH values. But between pH values 13.34 and 13.54 the band gap increased drastically.

7.4 Conclusion

In summary, the SEM images showed the impact of pH values on the preparation of the ZnO using ethanol, methanol and water. Various ZnO nanostructures were observed with different pH values at an annealing temperature of 600 °C. PL emission spectra were also taken and have showed the optical properties of ZnO when prepared with various solvents. It was observed that all ZnO samples showed a strong broad blue emission at 428 nm and a weak shoulder in the UV region. From the XRD pattern we were able to determine the grain sizes and the lattice parameters. The samples gave the three major peaks of which were the same as of the JCPDS 36-1451 and 79-0207. The UV-vis absorption was observed at different pH level together with the direct band gap. The effects of pH value were observed on the ZnO prepared using various solvents.

References

[1] M. H. Huang *et al.*, *Science* **292** 1897-1899 (2001)

[2] G. D. Mahan, *J. Appl. Phys.* **54** 3825-3832 (1983)

[3] K. Keis, E. Magnusson, H. Lindstrom, S. E. Lindquist, and A. Hagfeldt, *Sol. Energy Mater. Sol. Cells* **73** 51-58 (2002)

[4] D. Gruber, F. Kraus, and J. Muller, *Sens. Actuators B* **92** 81-89 (2003)

[5] K. J. Lee, MSc thesis, Texas A&M University (2005)

[6] D. Vernardou, G. Kenanakis, S. Couris, E. Koudoumas, E. Kymakis, N. Katsarakis, *Thin Solid Films* **515** 8764-8767 (2007)

[7] S. S Alias, A. B. Ismail, A. A Mohamad, *J. Alloys and Comp.* **499** 231-237 (2010)

[8] A. Chittofrati, E. Matijevic, *Colloids Surf.* **48** 65-78 (1990)

[9] D. C. Reyolds, D. C. Look, B. Jogai and H. Morkoç, *Solid state Commun.* **101** 643-646 (1997)

[10] V. A. L. Roy, A. B. Djurišić, W. K. Chan, J. Gao, H. F. Lui and C. Surya, *Appl. Phys. Lett.* **83** 141-143 (2003)

[11] A. B. Djurišić, Y. H. Leung, W. C. H. Choy, K. W. Cheah, and W. K. Chan, *Appl. Phys. Lett.* **84** 2635-2637 (2004)

[12] L. E. Greene, M. Law, J. Goldberger, F. Kim, J. C. Johnson, Y. Zhang, R.J. SayKally and P. Yang Angew, *Chem. Int. Ed.* **42** 3031-3034 (2003)

[13] J. Wang, L. Gao, *Solid State Commu.* **132** 269-271 (2004)

[14] A. Sarkar, S. Ghosh, S. Chaudhuri and A. K. Pal, *Thin Solids films* **204** 255-264 (1991)

CHAPTER 8

SUMMARY AND CONCLUSION

8.1 Thesis summary

In this report the ZnO nanoparticles was synthesized and characterized by using the sol-gel process. The ZnO nanoparticles using PEG were synthesised with an annealing temperature of 150 °C with ethanol as a solvent. Once again the ZnO nanoparticles and the ZnO were synthesized encapsulated with a polymer PVP. The comparison of ZnO nanoparticles properties was synthesised at different temperatures by using various solvents. The last part of this report was the influence of pH value on the material properties of the ZnO nanostructures using various solvents at constant temperature.

All these samples were characterized using different techniques. The morphology of the nanoparticles was observed by a Shimadzu Superscan SSX-550 system scanning electron microscope (SEM) operated at 20 kV equipped with energy dispersive X-ray spectroscopy (EDS). Optical absorption was performed on a Perkin Elmer Lamb 950 UV-visible spectrophotometer (UV). The X-ray diffraction (XRD) patterns were recorded to characterize the phase and crystal structure of the nanoparticles using a D8 Bruker Advanced AXS GmbH X-ray diffractometer (XRD), room temperature photoluminescence (PL) of the samples was measured, using a He–Cd laser (325 nm) as excitation sources.

In the preparation of the ZnO nanoparticles encapsulated with PVP, the PL characterization showed a broad emission at around 449 nm and at around 530 nm. This was due to the various molar masses of PVP which was added on the ZnO. The XRD for the ZnO nanoparticles gave the pattern that corresponded to the ZnO wurtzite. The SEM image exhibited the agglomeration of particles which was influenced by the overlapping of small particles. There was a slight shift on the UV absorption spectra which were brought by the addition of the molar masses of the PVP.

The surface morphology and the photoluminescence (PL) properties of ZnO depended highly on the synthesis process and PEG encapsulation. The absorption edges of these ZnO nanoparticles were shifted by additions of the PEG polymer. The PL emissions from the ZnO nanoparticles dispersed in water have been measured under 325 nm UV light excitations. The photoluminescence (PL) characterization of the ZnO nanostructures exhibited a broad emission in the visible range with maximum peak at 450 and/or 560 nm. The X-ray diffraction (XRD) spectra for ZnO nanoparticles showed that all the peaks corresponding to the various planes of wurtzite ZnO indicated the formation of a single phase.

The photoluminescence spectra varied with different temperatures with respect to the solvents used to prepare the ZnO nanoparticles. The UV-vis absorption exhibited various absorption peaks for various solvents when annealed at different temperatures. The ZnO prepared using water gave the nanorods, while ZnO prepared using ethanol showed the clustered nanorods at a temperature of 300 °C and monodispersed particles when annealed at a temperature 600 °C. The SEM image of the ZnO prepared using methanol showed the agglomerated ZnO nanoparticles both at temperatures 300 and 600 °C. Agglomeration effect was very prominent in aqueous media as compared to organic solvents because organic solvents have better dispersing ability [7].

The characterization of the ZnO nanoparticles prepared by varying the pH values of the different solvents. The PL showed strong broad blue emission. The SEM images for the ZnO prepared using ethanol and methanol gave agglomerated spherical ZnO particles which are closely packed together. SEM images of the ZnO prepared using water presented the agglomerated particles at pH 10.06 and a decrease on the particle growth at the pH value of 13.54. The XRD pattern for all ZnO nanostructures prepared using ethanol; methanol or water exhibited the major peaks which has characteristics as of those of the ZnO wurtzite structure. The XRD pattern ZnO prepared using ethanol showed a decrease on the intensity peak with an increase on the pH value. The same has occurred with the XRD patterns of the ZnO prepared using methanol and water. It was observed from the UV absorption of the ZnO using different solvents that the band gaps for all the samples were determined to be larger than that of ZnO bulk.

8.2 Future Work

Different nanostructures of ZnO such as nanoparticles and nanorods have been investigated in this report. ZnO can form a number of morphological structures, including particles, rods (wires) and can be investigated. Preparation of ZnO using a CBD method can be looked at. The investigation might also include the ways on how to control the agglomeration of the ZnO particles, effects of the method used to prepare these particles. The preparation of ZnO annealed at lower temperatures can also be looked into. The synthesis and the characterization of the ZnO doped with different transition metals could be investigated and the impact of these metals on the properties of the ZnO. This can be done using a sol-gel spin coating method.

Publications

- M A Tshabalala, B F Dejene and H C Swart, Synthesis and characterization of the ZnO nanoparticles and the polyvinyl pyrrolidone (PVP) encapsulated ZnO nanoparticles, Pretoria 2011. **Submitted July 2011.**

- M A Tshabalala, B F Dejene and H C Swart, Synthesis and characterization of ZnO nanoparticles using Polyethylene Glycol (PEG), Accepted (2011) & Published by Elsevier B.V. doi:10.1016/j.physb.2011.09.113

Conferences

- M A Tshabalala, B F Dejene and H C Swart, Synthesis and characterization of ZnO nanoparticles using Polyethylene Glycol (PEG).

4th South African Conference on Photonic Material, hosted by UFS, Kariega Game Reserve, 2 – 6 May 2011.

- M A Tshabalala, B F Dejene and H C Swart, Synthesis and characterization of the ZnO nanoparticles and the polyvinyl pyrrolidone (PVP) encapsulated ZnO nanoparticles.

56th Annual Conference of the South African Institute of Physics (SAIP), hosted by UNISA, St Georges Hotel and Convention Centre, Pretoria, 12 – 15 July 2011.